Research Square

Preprints are preliminary reports that have not undergone peer review.
They should not be considered conclusive, used to inform clinical practice,
or referenced by the media as validated information.

# CRISPR-based epigenome and genome editing reveal novel roles for PLEC in cartilage biology, mechanobiology, and response to inflammation

**Antony K Sorial**
Washington University School of Medicine
**Zainab Harissa**
Washington University School of Medicine
**Nancy Steward**
Washington University School of Medicine
**Yulia Kehayova**
Newcastle University
**Alireza Savadipour**
Washington University School of Medicine
**Neda Rashidi**
Washington University School of Medicine
**Yuseon S. Kim**
Washington University School of Medicine
**Jack B. Roberts**
Newcastle University
**Guillaume A. Aubourg**
Newcastle University
**Matt J. Barter**
Newcastle University
**Sarah J. Rice**
University of Manchester
**Wenjia Feng**
Washington University
**Bo Zhang**
Washington University
**David J Deehan**
Freeman Hospital
**Gerhard Wiche**
University of Vienna

**Farshid Guilak**

guilak@wustl.edu

Washington University School of Medicine

---

**Research Article**

**Keywords:** Osteoarthritis, Cartilage, Mechanobiology, Mechanotransduction, Mechanoinflammation, Cytoskeleton, Plectin, Chondrogenesis

**Posted Date:** August 18th, 2026

**DOI:** https://doi.org/10.21203/rs.3.rs-10171592/v1

**License:** This work is licensed under a Creative Commons Attribution 4.0 International License. Read Full License

**Additional Declarations:** Competing interest reported. Unless stated, the author has no competing interest to declare. FG is a shareholder and employee of Cytex Therapeutics Inc.

# CRISPR-based epigenome and genome editing reveal novel roles for *PLEC* in cartilage biology, mechanobiology, and response to inflammation

Antony K Sorial[1,2,3,4], Zainab Harissa[1,2,3], Nancy Steward[1,2,3], Yulia Kehayova[4], Alireza Savadipour[1,2,5], Neda Rashidi[1,2,5], Yuseon S. Kim[1,2,3], Jack B. Roberts[4], Guillaume A. Aubourg[4], Matt J. Barter[4], Sarah J. Rice[6], Wenjia Feng[7], Bo Zhang[7], David J Deehan[8], Gerhard Wiche[9], Farshid Guilak[1,2,3]

[1]Department of Orthopedic Surgery, Washington University School of Medicine, St. Louis, MO, USA
[2]Shriners Hospitals for Children - St. Louis, MO, USA
[3]Department of Biomedical Engineering, Washington University, St. Louis, MO, USA
[4]Biosciences Institute, Newcastle University, Newcastle upon Tyne, UK
[5]Department of Mechanical Engineering and Material Science, Washington University, St. Louis, MO, USA
[6]Division of Musculoskeletal & Dermatological Sciences, University of Manchester, UK
[7]Department of Developmental Biology, Washington University, St. Louis, MO, USA
[8]Freeman Hospital, Newcastle upon Tyne, UK
[9]Department of Biochemistry and Cell Biology, Max Perutz Labs, University of Vienna, Austria

**Address for correspondence:**
Farshid Guilak, Ph.D.
Couch Biomedical Research Bldg., Room 3121
Campus Box 8233
Washington University
Saint Louis, MO 63110
Email address: guilak@wustl.edu

**Keywords**: Osteoarthritis, Cartilage, Mechanobiology, Mechanotransduction, Mechanoinflammation, Cytoskeleton, Plectin, Chondrogenesis

## Declarations

### Ethics approval and consent to participate

For patient cartilage samples, ethical approval was obtained from the National Health Service Health Research Authority (NHS-HRA), Research Ethics Committee Reference 19/LO/0389. All patients who donated tissue undertook formal written consent at the time of surgery.

### Consent for publication

Not applicable

### Availability of data and materials

All data underlying the figures are available upon request.

### Competing interests

Unless stated, the author has no competing interest to declare. FG is a shareholder and employee of Cytex Therapeutics Inc.


### Funding

Unless stated, the authors have no funding to declare relevant to this work. AKS: Wellcome Trust 4Ward North, Royal College of Surgeons of England (RCS Eng) Shears Fellowship, RCSEng / UK-US Fulbright Commission Award, GW: Collaborator AR080409, Wellcome 4Ward North, FG: Shriners Hospital's for Children, National Institutes of Health (AR080409, AG15768, AG46927, AR080902, AR072999, AR073752, AR074992). ZH: NIH AR079283).


### Authors' contributions

AKS/FG developed the concept of the study; AKS/SJR designed the methylation studies; AKS/MB/FG developed the iASC-s9c9 cell line; AKS, ZH, NS, YK, AS, NR, YSK, JBR, GAA undertook experimental work; AKS/WF/BZ analysed/interpreted RNAseq; AKS/ZH analyzed other data and generated figures; DJD assisted with project funding/design and critical review for intellectual content; AKS/GW designed plectin experiments, GW provided antibodies, protocols and experimental reagents; AKS/ZH/FG wrote the manuscript; AKS/FG acquired funding for the study, all authors edited and approved the final manuscript.


### Acknowledgements

Nil.

## Abstract

### Background

Osteoarthritis (OA)-associated single nucleotide polymorphism (SNP) rs11780978 has previously been associated with differential methylation at sites within *PLEC* gene and differential expression of *PLEC* in multiple joint tissues, including cartilage. We undertook experiments to identify novel differential methylation sites and used epigenome editing to link rs11780978 associated differential methylation to *PLEC* expression. Here, we established a novel pipeline using immortalized human chondrogenic cells to determine the role of *PLEC*. CRISPR based genome editing was employed to replicate plectin deficiency followed by deep phenotyping through cartilage development (chondrogenesis), and homeostasis.

### Methods

Methylation quantitative trait loci (mQTL) analyses of novel CpGs were undertaken. Epigenome editing was employed to modulate methylation at CpGs of interest and expression of genes of interest was screened by qPCR. A novel, highly chondrogenic CRISPR based cell line was used to develop a *PLEC*-knockout and CTRL line. Cells underwent chondrogenesis and were phenotyped by qPCR as well as staining/immunohistochemistry for matrix components. Cells were challenged with mechanical and mechano-inflammatory stimuli and phenotyped by high depth RNA sequencing.

### Results

Two previously described and four novel mQTLs were replicated in human OA cartilage. The six mQTLs were targeted with epigenome modulation which prioritised *PLEC* for further study. Plectin editing was efficient at the DNA, mRNA and protein level and was maintained throughout chondrogenesis and mechano-inflammatory challenge. Plectin deficiency was associated with molecular phenotypes, including reducing anabolism following chondrogenesis. Deep phenotyping of the chondrocyte response to loading and combined mechano-inflammation identified genes and pathways of interest intersecting with plectin deficiency.

### Conclusions

We report a functional pipeline to test a non-coding OA SNP from epigenome editing, through genome editing and downstream deep phenotypic characterisation of genes of interest in in vitro cartilaginous model systems replicating the mechano-inflammatory environment. This system enabled us to identify multiple novel links between the functional region, plectin and chondrocyte biology and mechanobiology. These data enhance our knowledge on plectin biology and provide new pathways of interest for future study.

## Introduction

Osteoarthritis (OA) is the most common form of arthritis and the leading cause of disability globally[1]. OA occurs in synovial joints, most commonly affecting the hand, hip, and knee[1]. Focal loss and subsequent degeneration of articular cartilage is characteristic of OA; however, it is increasingly understood that the disease is multifactorial, affecting multiple tissues within the joint, with a well-established inflammatory component contributing to disease development and progression[2]. The etiology and pathogenesis of primary OA involves the contribution of multiple risk factors, including increasing age[3], female sex[4], obesity[4], and anatomical variation (such as knee malalignment[5], hip dysplasia[6, 7], and deformity[6]). The advent of powerful genome-wide association studies (GWAS) has facilitated the identification of disease-associated single-nucleotide polymorphisms (SNPs), establishing a crucial role for common genetic variation in the development of OA [8]. Indeed, it is now estimated that nearly half of OA risk is genetically associated [9].

Most OA-associated SNPs reside in non-coding regions of the genome and tend to confer their effects by secondary epigenetic mechanisms such as DNA methylation (DNAm), chromatin modifications, and non-coding RNAs. The most well-characterized of these mechanisms in the pathogenesis of OA is DNA methylation, which is commonly associated with gene silencing through transcriptional repression[10]. A growing body of evidence has linked OA-associated SNPs to DNAm at multiple locations within the genome, in close proximity to potentially pathogenic genes associated with OA [9, 11-18]. Correlations between SNP genotype and methylation levels at CpG sites are termed methylation quantitative trait loci (mQTLs). Many OA-associated SNPs have been demonstrated to act as mQTLs in patient tissues [11-13, 18, 19], providing an intermediary mechanism useful for identifying target genes affected by these variants.

There is extensive evidence for OA as a “whole joint” disease[20], and perhaps, fitting

the criteria for a "whole body" disease[21], with epigenetic effects seen in cartilage, fat pad, synovium and blood mQTL analyses[12, 13]. Cartilage is the main load-bearing and articulating tissue in the joint, in which chondrocytes constitute the main residing cell type [22, 23]. Subsequently, the reproducible and extensively described process of chondrocyte development, maturation, and extracellular matrix (ECM) deposition, known as chondrogenesis, presents an opportunity to study the role of OA risk genes *in vitro* [24-26].

We have previously identified and characterized rs11780978 [11, 13], a G>A polymorphism with a minor allele frequency of 0.42, significantly associated with hip OA ($P = 1.98 \times 10^{-9}$) [27]. This SNP resides on chromosome 8, in an intron of the *PLEC* gene encoding plectin, a large, complex, multi-functional cytoskeletal protein [28]. Our previous data suggest a potential role for *PLEC* and another gene on Chromosome 8, *GRINA,* in the OA susceptibility associated with rs11780978, potentially mediated through DNAm in cartilage[11, 13]. Genetic and epigenetic data from the analyses suggested that *PLEC* may be the strongest candidate gene for further investigation[11, 13].

*In vivo*, following embryonic development, cartilage is subjected to a lifetime of stimuli, including mechanical load, inflammation, and injury. Understanding how genetic risk factors for OA can interact with the cartilage microenvironment in response to physiological and pathological conditions is therefore crucial in studying disease development, progression, and identifying targets for therapeutics. To understand the contribution of *PLEC* and other OA risk genes, we aimed to develop an *in vitro* system that could replicate the effects of genetic risk factors on growth, maturation, and environmental exposure (i.e., cytokines, mechanical loading) throughout the course of chondrocyte differentiation and maturation. To investigate chondrogenic phenotypes, we employed a highly chondrogenic immortalized adipose stem cell (iASC-s9) line[29]. This line supports extensive passaging, without requiring supplemental growth factors for differentiation, using protocols identical to those used for primary ASCs or

bone marrow-derived mesenchymal stem cells (BM-MSCs)[30].

The goal of this study was to further assess rs11780978 associated mQTLs and apply *in vitro* genome and epigenome editing techniques to ascertain the molecular function of the risk allele on *PLEC*. We also aimed to develop and test a novel *in vitro* system replicating the *in vivo* mechano-inflammatory environment as a conduit to understand the role of plectin deficiency in cartilage development and the response to environmental factors.

## Materials and Methods

### Patients and base cell lines

Cartilage samples were collected from patients undergoing hip and knee arthroplasty for primary OA. Nucleic acids were extracted from cartilage, TC28a2 chondrocyte-like cell line and immortalised adipose derived SOX9 overexpression line (iASC-s9) by Purelink Genomic DNA mini-kit (Invitrogen) as previously described [14]. TC28a2 was established prior to this work by transfecting primary cultures of costal cartilage from a 15-year-old female [31, 32], iASC-s9 was also developed previously [29]. Detailed data on patient demographics is included in Table S1.

### Genotyping

DNA from patient cartilage samples, TC28a2 and iASC-s9 cell lines was genotyped at rs11780978 via restriction fragment length polymorphism (RFLP) as previously described [11, 13]. All samples were genotyped and randomly distributed to methylation experiments to ensure an equal spread of genotypes across the CpG assays.

### Design and validation of pyrosequencing assays to target CpGs

DNAm analysis at cg19405177 and cg14598846 was undertaken as previously described [11, 13]. For novel CpGs, assays were generated using Pyromark Assay Design

Software (Qiagen) [14]. In brief, DNA sequences of 100 bp upstream and downstream of each CpG were exported from human genome 19 (hg19) of the University of California Santa Cruz (UCSC) Genome Browser and imputed into the assay design software. Assays with the highest quality score were purchased as oligonucleotides from Integrated DNA Technologies (IDT). Where 200 bp of DNA sequence did not yield assays, the length of DNA was increased to improve assay design. Despite altering design parameters, novel CpG cg01870834 was not targetable by pyrosequencing. For the remaining novel CpGs, 500 ng of genomic DNA was bisulfite converted by EZ DNA Methylation kit (Zymo Research) and amplified in duplicate using the Pyromark PCR kit (Qiagen), as previously described[11, 13].

4 assays targeting novel CpGs (cg20784950 in cluster 1, cg04255391 and cg10299941 in cluster 2 and cg07212837) did not amplify or amplified with non-specific banding. For each, an alternative assay was designed. PCR optimisation was undertaken as per manufacturer instructions. Despite multiple attempts, assays consistently failed quality control (QC) checks and were therefore abandoned. The seven CpGs analysed were: cg19405177/cg24891660 (original cluster 1 and a novel CpG at cluster 1), cg07427475, cg02331830, cg14598846, cg23299254 (all belonging to cluster 2), and the novel CpG located between the first exons of *PLEC*, cg21511203. Methylation analyses were undertaken as previously described [11, 13]. *P*-values were calculated for genotype-methylation correlations (mQTLs) by a Kruskal-Wallis test [11, 13]. Pyrosequencing assays are presented in Table S2.

**Development of a chondrocyte-like inducible dCas9-TET-1 cell line**

An a previously developed, inducible, puromycin selectable TC28a2-dCas9-TET-1 cell line was utilized [12].

## In silico CRISPR design

Based on previous data [12, 15], CpGs were targeted with a single guide RNA (gRNA), with a 5'-3' direction toward the CpG site, located 15-50 bp away. For each CpG, DNA sequences 50-100 bp up and downstream were extracted from the hg19 genome browser and imputed into the IDT gRNA design tool. gRNA designs were identified and scored based on direction and distance from the CpG site, prioritizing high on-target activity and low off-target activity. gRNAs and tracrRNA from IDT were used as previously described [13]. gRNA locations were verified for each CpG using the sequence alignment tool (UCSC). Non-targeting gRNA (NTgRNA, control) was purchased from IDT and verified using UCSC. gRNA sequences and IDT assay references are available in Table S3.

## Cell culture, induction and transfection

TC28a2-dCas9-TET-1 cells were cultured as previously described [12], with selection for the CRISPR plasmid in complete medium supplemented with 1µg/ml puromycin[12]. Each gRNA or the NTgRNA (Table S3) was annealed to tracrRNA to form duplexes as previously described[12, 13]. Cells were seeded at 100,000 cells/well in 6 well plates (VWR), allowed to adhere for 24 hr in complete medium without puromycin, followed by induction of dCas9-TET-1 expression with 1µg/ml doxycycline.

## Nucleic acid extraction of cells in monolayer

DNA was extracted by Purelink Genomic DNA mini kit (Invitrogen). RNA was extracted from pellets using the NucleoSpin RNA kit (Macherey–Nagel) as per manufacturer instructions with on-column manufacturer DNase treatment.

## Detection of dCas9-TET-1 induced methylation modulation

DNA extraction, bisulfite conversion, and DNAm analysis by pyrosequencing were undertaken as previously described [13]. DNAm values of NTgRNA (control) were compared to gRNA for each CpG. Data were analyzed and visualized in GraphPad PRISM.

## Quantitative gene expression following methylation modulation

cDNA synthesis was undertaken using Superscript IV (Invitrogen) following the manufacturer's protocol, and gene expression analyses were undertaken as described previously [15]. In summary, comparison was made to three housekeeper genes (*18S*, *GAPDH*, *HPRT1*) using the $2^{-\Delta Ct}$ method. Housekeepers and genes of interest (GOI) were measured using three technical replicates for each biological replicate. IDT predesigned assays, which targeted all transcripts of *PLEC* (HS.PT.58.3012276, exon 11-13), *GRINA* (HS.PT.58.39790981.g, exon 4-5) and *PARP10* (Hs.PT.58.21152609, exon 9-10) were used per manufacturer instructions. For fold-change gene expression changes, each well of treatment (gRNA) was paired to a well of control (NTgRNA) and a paired t-test was employed as described previously [15].

## dCas9-DNMT3a delivery system

The dCas9-DNMT3a-EGFP plasmid (71666, S. pyogenes dead Cas9 fused with the catalytic domain of human DNA methyltransferase 3A) was purchased from Addgene and column-purified plasmid DNA was validated as previously described [15]. Identical gRNA sequences (Table S3) were ordered as single-stranded oligonucleotides, annealed, and ligated into the pdCas9-DNMT3a-EGFP as previously described [14, 33], with confirmation of gRNA ligation to plasmid by Sanger sequencing. Detection of methylation changes was undertaken using primers in Table S2 with comparable protocol to mQTL analyses.

**TC28a2-dCas9-DNMT3a-EGFP cell culture and nucleofection**

Cells were cultured as described above in the absence of puromycin, as they did not contain the puromycin resistance gene. 1 x $10^6$ cells per replicate were nucleofected with 5µg (1µg/µl) of concentrated plasmid DNA in an Amaxa 4D-Nucleofector (Lonza) in cell line solution SF with pre-optimized programme EH-100. GFP was visualized at 24 hr to confirm transfection, and cells were allowed to expand until confluent in a T-25 flask.

**iASC-s9 cell line culture**

Cells were cultured and expanded as previously described [29]. In brief, cells were grown in Mesenchymal Stem Cell Basal Medium (ATCC, PCS-500-030) with 10 ml of supplement and 6 ml of L-Alanyl-L-Glutamine (both components of ATCC, PCS-500-040). 0.2 mg/ml G418 (Sigma, G8168) was added to select for human telomerase reverse transcriptase (hTERT).

**Nucleic acid extraction from cell pellets**

Cell pellets were harvested, washed in PBS, and snap-frozen in dry ice, and stored at -80 °C. DNA and RNA were simultaneously extracted from each pellet using the DNA/RNA purification kit (Norgen, 48700) with an on-column DNase digestion (Norgen, 25710). RNA was quantified and 500ng was reverse transcribed using Superscript IV reverse transcriptase and buffer (Invitrogen). The remaining DNase-treated RNA (at least 900 ng/sample) was stored at -80 °C for RNA-Sequencing (RNAseq).

**Quantitative gene expression in iASC-s9**

Gene expression in iASC-s9 was measured as described, with the addition of the following gene assays purchased from IDT: *SOX9*, *COL2A1*, *COL1A1*, *COL10A1* and *ACAN*. Sequences are available in Table S4.

## Development and validation of an inducible CRISPR-Cas9 chondrogenic culture system

An inducible, selectable CRISPR approach was chosen as previous work had demonstrated that sustained overexpression of Cas9 attenuated chondrogenesis (unpublished data). Lentivirus was produced by transfecting HEK-293T cells with inducible Cas9 (iC9) plasmid PCW-Cas9 with puromycin selection (Addgene plasmid #50661), together with packaging plasmids PCMV-VSV-G (Addgene plasmid #8454, deposited by Bob Weinberg) and psPAX2 (Addgene plasmid #12260, deposited by Didier Trono). Virus-containing culture media was collected every 24 hr for 3 days and concentrated (10x) with Clontech Lenti-X Concentrator in PBS (Takara). iASC-s9 were expanded and plated at 50-60% confluence in 10 cm culture dishes. Next, ~ 300,000 cells were transduced with the lentivirus-containing 8μg/ml polybrene in PBS. Based on an optimisation kill curve, a final concentration of 0.9 μg/ml of filter-sterilized puromycin was used to select for the transduced cells. These cells were designated as iASC-*SOX9*-Cas9 (iASC-s9c9). Doxycycline-inducible expression of Cas9 protein was confirmed via immunoblotting using a Cas9 antibody (7A9-3A3; Cell Signalling Technology).

## Generation of *PLEC* knockout (*PLEC*-KO) iASC-s9c9 cell line

At each passage, cells were allowed to adhere for 24 hr in complete medium, prior to supplementation with 0.9 μg/ml puromycin. Prior to transfection, cells were trypsinized, harvested, and cultured in T75 flasks in media without puromycin. To induce Cas9 expression, complete medium containing 1 μg/ml of sterile filtered doxycycline was added. A paired guide approach using two previously validated gRNAs targeting exon 3 of *PLEC* [13] was employed. In brief, previously validated gRNA sequences [13] that would generate a 26 bp frameshift deletion of exon 3 of *PLEC* (primers 5’ - CTGTATGAAGACCTCCGCGA - 3’ and 5’ - CCCCGAGAGGACCTCCAGCA - 3’) were purchased as synthetic Alt-R® CRISPR-Cas9 crRNAs alongside Alt-R® CRISPR-Cas9 tracrRNA (Integrated DNA Technologies). To

generate a *PLEC* knockout cell line (iASC-s9c9-*PLEC*-Knockout; *PLEC*-KO) crRNAs were annealed to tracrRNA in a 1:1:2 ratio at 95 $^{o}$C for 5 min. For *PLEC* control (iASC-s9c9-*PLEC*-CTRL) a commercially available non-targeting crRNA sequence was used (5'-CGTTAATCGCGTATAATACG - 3'). Deletion and control mixes were separately combined with Dharmafect1 (Dharmacon) in serum-free media (PCS-500-030, ATCC) to produce a transfection mix. Cells were transfected for 48 hr, washed in PBS, and allowed to recover in complete medium without puromycin.

**Validation of genome editing**

DNA and RNA were extracted from cell pellets using the RNA/DNA purification kit (Norgen, 48700). Protein was extracted using the NucleoSpin RNA-Protein Kit (Macherey–Nagel) and quantified using a protein quantification kit (Macherey–Nagel). Deletion of the target region was confirmed by end-point PCR of DNA using primers flanking the guides (primers 5' – GAGGGGTTGAGCTGGATTCC - 3' and 5' – CCAGCACCCACTCTGTAGAT - 3'). For Sanger sequencing of DNA, flanking PCR product was run on a 3% agarose gel, and the knockout or CTRL band was excised under ultraviolet (UV) light. Gel bands from CTRL and *PLEC*-KO were digested, and DNA extracted using the QIAquick Gel Extraction Kit (Qiagen). DNA editing was confirmed by gel visualization and by Sanger sequencing of the excised PCR products.

For confirmation of plectin depletion, up to 15 μg of total protein was resolved on NuPAGE™ 3-8% Tris-Acetate Protein Gels in 1 x NuPAGE™ Tris-Acetate SDS Running Buffer (Invitrogen). Protein was transferred through a semi-dry transfer using an iBlot™ 2 nitrocellulose mini transfer stack and iBlot™ 2 device (Thermo Fisher). A custom program (P3, 13 minutes) was used due to the high molecular weight of plectin. Blots were probed with anti-plectin guinea pig antiserum (GP21, Progen)/goat anti-guinea pig (AB6908, Abcam) and anti-GAPDH (#5174, Cell Signalling Technologies)/anti-rabbit IgG (#7074, Cell Signaling

Technologies) as a loading control. To confirm maintenance of plectin deficiency, protein was collected at timepoints from P1-P6 in monolayer, at all pellet chondrogenic timepoints, prior to seeding in agarose and following agarose chondrogenesis.

**Chondrogenic differentiation of iASC-s9c9 CTRL and *PLEC*-KO**

The following timepoints were chosen day 0- baseline; day 3- induction of *SOX9* and initiation of chondrogenesis; day 7- middle to maximal chondrogenesis; day 21- maximal chondrogenesis to early hypertrophy; day 42-hypertrophy.

Matched passage (P2 after editing) CTRL and *PLEC*-KO cells were thawed and expanded to a cell density of ~ 2000 cells/cm$^2$. Multiple inductions of chondrogenesis were undertaken using matched cryovials, as previously described [29]. In brief, both lines were simultaneously expanded, harvested, and counted using a Countess 2 electronic cell counter (Invitrogen), with trypan blue to determine cell viability. Pellets were formed by centrifuging 400,000 cells at 200 x g for 5 min in sterile conical-bottomed 96-well plates (Alkali Scientific, MPD26-S). Pellets were differentiated in standard chondrogenic media[29]. Media was changed twice weekly.

**Agarose culture**

CTRL and *PLEC*-KO cells were expanded, harvested and seeded in 2% agarose at 20 x $10^6$ cells/ml. 3.37mm cylindrical agarose constructs were punched out using a Miltex Biopsy Punch (Ted Pella) and cultured in chondrogenic medium for 42 days.

**Nucleic acid and protein extraction from pellet chondrogenesis**

Chondrogenic pellets were collected at d7, d21, and d42, washed in PBS, and transferred to 2 ml screw-top molecular grinding tubes (Sarstedt) containing autoclaved Zirconia grinding beads (Biospec) and DNA/RNA extraction buffer SKP (Norgen)

supplemented with 1% β-Mercaptoethanol (BME). Due to the dense extracellular matrix (ECM) produced at d21 and d42, 2-4 pellets were combined into one tube to maximise DNA and RNA yield. For protein, 4 x d42 pellets/tube were snap frozen in buffer RP1 (Macherey-Nagel) supplemented with 1% BME. To homogenize chondrogenic pellets a mini bead beater (Biospec) was used as previously described [29]. DNA and RNA were quantified by spectrophotometry (Nanodrop ND-1000). Protein was quantified by protein quantification kit (Macherey–Nagel).

**cDNA synthesis and qPCR of chondrogenesis**

300-600 ng of RNA was reverse transcribed to cDNA by Superscript VILO Master mix (Life Technologies) as per manufacturer instructions. cDNA was diluted to 5 ng/µl and 10 ng/reaction was analysed in duplicate, normalizing to housekeeping genes 18s ribosomal RNA[29] and *GAPDH*. Identical qPCR primers (Table S4) were combined with Fast SYBR Green Master Mix (Applied biosystems).

**Biochemical analysis of cartilaginous matrix production in pellets and agarose constructs**

Pellets and agarose constructs were digested in 200 µl papain solution and GAG/DNA ratio calculated as previously described[34].

**Histology and immunohistochemistry (IHC) in pellet chondrogenesis**

Pellets were fixed in 10% neutral buffered formalin for 24 hr and transferred to 70% ethanol, dehydrated, and embedded in paraffin wax. Pellet blocks were sectioned at 8 µm thickness and stained for proteoglycans and cell nuclei according to the Safranin-O and hematoxylin protocol[34]. To assess anabolism (Type II Collagen) and hypertrophy (Type X Collagen) IHC was undertaken[34]. In brief, samples were labelled for 1 hr with the primary antibodies Type II Collagen (1:10 Iowa #II-II6B3-s) or Type X Collagen (1:200 Sigma

#C7974), and for 30 min with the secondary antibody goat anti-mouse (1:500, Abcam #97021). Safranin O and IHC Images were taken using an Olympus VS120 microscope (VS120-S6-W).

**Inflammatory challenge in pellet chondrogenesis**

An inflammatory challenge with cytokine Interleukin-1 beta (IL-1β) was undertaken to assess the response of CTRL and *PLEC*-KO chondrogenic pellets to inflammation. At d42, pellets were treated with 1 ng/ml Recombinant Human IL-1 beta/IL-1F2 protein (R&D Systems, 201LB005) for 72 hr or left untreated to serve as a control for each cell line.

**Atomic force microscopy (AFM) of plectin deficient pellets and chondrocytes**

AFM in pellets was undertaken as previously described [35, 36]. d42 CTRL and *PLEC*-KO IL-1β treated or untreated pellets were loaded as in [35]. For single cell AFM, d42 chondrogenic pellets from each line were digested with 0.04% Type II collagenase solution (C5138, Sigma-Aldrich) in DMEM/F12 for 1-2 hr and chondrocytes frozen for downstream analysis. 72 hr prior to testing, matched cryovials of chondrocytes were plated and allowed to recover. On the day of testing, cells were trypsinised and plated for 2.5 hr prior to loading. Cells were loaded to 500 nN using an AFM (Asylum Research MFP-3D) with tipless cantilevers (k = 6.2 N/m; MikroMasch) and analyzed to calculate deformation, overall fluorescence and the number of responders as previously described [36].

**Dynamic mechanical compression in iASC-s9c9 constructs**

A custom-designed hydraulic mechanical compression device was used to apply dynamic, unconfined compression to agarose constructs in a controlled environment (37ºC, 5% $CO_2$). Sinusoidal compression of 24 agarose constructs (12 CTRL and 12 *PLEC*-KO) was performed simultaneously using a closed-loop displacement feedback system to mimic physiological loading as previously described [37, 38]. To validate loading and response to

inflammation, a panel of previous reported mechanoresponsive genes (*PTGS2, BMP, INHBA, FGF1 and NFATC1* [29, 37]) and an inflammatory pathway gene (*IL6)* were assessed by qPCR.

**Assessment of response to load, inflammation, and load in the presence of inflammation (mechano-inflammatory model)**

To assess the role plectin plays in the chondrocyte response to load, inflammation, and load in the presence of inflammation, experiments were designed to replicate a mechano-inflammatory environment. To facilitate analyses assessing the effects of loading, the following experimental groups were designed: 1) Free swelling (FS) controls 2) response to anabolic load (dynamic compression, 3 hr duration, 1 Hz, 10% strain[29]). Second, to facilitate analyses to separately assess the effects of inflammation, and load in the presence of inflammation, the following experimental groups were designed: 1) Free swelling control for mechano-inflammatory model, 2) response to inflammation (72 hr IL-1β), response to mechano-inflammation (72 hr IL-1β challenge followed by 3 hr dynamic compression). This experimental design is demonstrated in Figure S1.

**Nucleic acid and protein extraction from agarose constructs**

Agarose constructs were harvested in Buffer SKP (Norgen) for DNA/RNA isolations, and buffer RP1 (Macherey-Nagel) for protein extractions, and snap-frozen in liquid nitrogen as previously described for pellet chondrogenesis. To minimize batch effects, all RNA extractions for sequencing were undertaken with identical lot-matched reagents, columns, buffers, and DNAse (Norgen).

**Bulk RNAseq**

To minimize DNA contamination prior to RNAseq, an off-column DNase kit (RNAse Free DNase I, Norgen) was used. DNase-treated RNA was delivered to Genome Technology Access Center (GTAC), McDonnell Genome Institute, Washington University in St. Louis.

RNA integrity was determined using Bioanalyzer or 4200 Tapestation (Agilent). Library preparation was performed with 500 ng to 1 μg of total RNA. Ribosomal RNA was removed by an RNase-H method using a RiboErase kit (Kapa Biosystems). mRNA was then fragmented in reverse transcriptase buffer and heated to 94 °C for 8 min then reverse transcribed to yield cDNA using SuperScript III RT enzyme (Life Technologies) and random hexamers. A second strand reaction was performed to yield ds-cDNA. cDNA was blunt-ended, had an A base added to the 3' ends, and Illumina sequencing adapters were ligated to the ends using a GTAC custom-designed in-house pipeline. Ligated fragments were then amplified for 12-15 cycles using primers incorporating unique dual index tags. Fragments were sequenced on an Illumina NovaSeq-6000 using paired-end reads extending 150 bases. Reads were processed using an in-house pipeline and open-source R packages. Briefly, raw reads were first trimmed by using cutadapt to remove low-quality bases and reads. Trimmed reads were then aligned to the human genome hg38 with GENCODE annotation v27 using STAR (v2.5.4) with default parameters. Gene and transcript expression were quantified by using featureCounts from the subread package (v1.6.3) and RSEM. Quality control assessments were made using RSeQC. Principle component analysis and differential expression analysis between groups were determined by using DESeq2 in the following cutoff (> 2-fold expression change, >3 samples with > 1 count per million (CPM), Benjamini corrected $P < 0.05$). Pairwise comparisons were made between experimental groups to determine differentially expressed genes (DEGs). All pipelines and custom scripts used in this study are available from https://github.com/Zhang-lab. To determine the effect of plectin deficiency, a second analysis was undertaken for each experimental group in which the response of the CTRL and edited line to each stimulus was assessed. This analysis was designed to provide a novel platform to identify specific DEGs within a line in response to various stimuli (Figure S2). Thus, identifying DEGs specific to or enhanced in plectin deficiency.

## Results

### rs11780978 associated functional region and the CpGs taken forward for analysis

In our past study, a 1 Mb region up and downstream of rs11780978 was used to detect genotype-methylation correlations, identifying nine mQTLs from cartilage DNA methylation array data[11]. Here, we performed an in-silico genome-wide mQTL analysis to determine whether additional, novel mQTLs with less significant effect sizes but closer to OA association SNPs could be detected. The size of the analysed region was reduced to 500kb upstream and downstream, reducing the number of CpGs tested, and allowing for a less stringent false discovery rate (FDR) threshold. This analysis identified three novel rs11780978 mQTLs: 1) cg24891660, approximately 2.4 kb 5' of cg19405177 (exon 28), in exon 24 of *PLEC* and with the same direction of effect (risk allele, A, correlates with higher methylation); 2) cg21511203 approximately 6.2 kb 5' of cg14598846, and around 15.8 kb 3' of rs11780978, lying between alternative first exons of *PLEC* and with the same direction of effect as cg19405177 and; 3) cg07212837, around 62 kb 5' of cg14598846, in close proximity to *GRINA* and with the same direction of effect as cg14598846, with the risk allele correlating with lower DNAm.

These three mQTLs, combined with the nine identified in our past study[11], yielded a total of 12 mQTLs to investigate. Cluster 1: cg19405177 and three other mQTLs (including a novel mQTL), Cluster 2: cg14598846, and five adjacent mQTLs and two individual mQTLs, cg21511203 and cg07212837 (Figure 1). Of the 12 remaining CpGs of interest, cg01870834 was not targetable by pyrosequencing, and 4 CpG assays, cg20784950 in cluster 1, cg04255391 and cg10299941 in cluster 2, and cg07212837, did not amplify or amplified with non-specific banding. After multiple validation attempts, these 5 CpGs were excluded, and the 7 CpGs reported in Table 2 were retained for the mQTL analysis.

**Six of the seven CpGs replicated as rs11780978 mQTLs including four novel replications**

DNA was extracted from 64 human cartilage samples from patients with a mean age of 65.6 (38-91). All samples were obtained from patients who underwent arthroplasty for primary OA. 33 (51.5%) were obtained from female patients, 36 (56.3%) were from the knee, and 28 (43.7%) from the hip. We also assessed methylation in chondrocyte-like cell line Tc28a2, and an immortalised adipose-derived stem cell line (iASC-s9), to inform downstream experiments assessing the role of the functional region.

Significant mQTLs were detected in cartilage at cg19405177 in cluster 1 and cg14598846 in cluster 2, as well as cg07427475, cg02331830 and cg23299254 in cluster 2, and novel CpG cg21511203 (Figure 2). For this study, only the array CpGs were reported, CpG assays; cg02331830, cg23299254 and cg21511203 captured additional adjacent CpGs all of which were significant mQTLs with comparable directions of effect (Figure S3). Methylation levels at cg24891660 did not correlate with genotype, with heterozygotes having lower methylation levels than homozygotes (Figure S4). Thus, cg24891660 was excluded from further analysis, as the relationship between methylation and genotype was inconsistent with that of a true mQTL.

**Modulating methylation at mQTL CpGs alters expression of *PLEC*, *GRINA* and *PARP10***

We aimed to experimentally provide evidence supporting a regulatory relationship at the locus by modulating methylation. Baseline methylation values at the CpGs of interest in two immortalized cell lines were first assessed. This included the human chondrocyte-like cell line TC28a2 and iASC-s9, which are heterozygous (GA) and homozygous (GG) respectively for the non-risk allele rs11780978. Of note, in cell lines methylation exhibited a site and line-specific pattern, with extremes of hyper and hypomethylation observed (Figure 2).

dCas9-TET-1 was employed to demethylate each of the replicated CpG sites. Demethylation was observed at all array CpGs after targeting with custom-designed gRNAs, compared to non-targeting gRNA, demonstrating successful use of the dCas9-TET-1 system (Figure 3A-F). The percentage of demethylation ranged from 3.2%, at cg21511203 (hypomethylated at baseline, Figure 3F), to 41.2% at cg23299254 (hypermethylated at baseline, Figure 3E). The single gRNA approach was effective at targeting the array CpG as well as adjacent CpGs captured on the assay. Generally, demethylation at the array CpG was equivalent to, or greater than other CpGs on the assay, suggesting that gRNA design (direction and location) was important in targeted demethylation (Figure 3A-F). In cg19405177, demethylation was observed at least 91 bp from the guide end point (the limit of the assay), suggesting potential demethylation outside of the measured range of all assays (Figure 3A).

In cluster 1, demethylating cg19405177 by 33.1% resulted in a reduction in *GRINA* and *PARP10* expression (Figure 3A). In cluster 2, a 5.8% reduction in cg07427475 resulted in significant decreases in *GRINA* and *PARP10* (Figure 3B), cg02331830 demonstrated 18.1% reduction with effects on *GRINA* (Figure 3C). Similarly, cg14598846 and cg23299254, which are in very close proximity, demonstrated effects on *PLEC* and *GRINA* (Figure 3D, E). Despite being hypomethylated, cg21511203 had a 3.2% reduction and appeared to reduce *PLEC* expression (Figure 3F). Of note, cg21511203 lies in the intron between the two first exons of *PLEC*.

Modulation at five CpGs (cg19405177, cg07427475, cg02331830, cg14598846, and cg23299254) was associated with a reduced expression of *GRINA*, modulation at three CpGs (cg14598846, cg23299254 and cg21511203) was associated with reduced expression of *PLEC*, and modulation at two CpGs (cg19405177 & cg07427475) was associated with reduced expression of *PARP10* (Figure 3A-F). A larger number of CpGs were associated with reduced *GRINA* expression, but the downregulation of *PLEC* was more significant (Figure 3A-F). Next,

dCas9-DNMT3a was used to target all six CpGs of interest using the same gRNAs as in the demethylation experiment. However, due to the baseline hypermethylation at 5 of the 6 CpGs (cg19405177, cg07427475, cg02331830, cg14598846, and cg23299254), pyrosequencing demonstrated no significant difference in methylation status (data not shown). Since methylation was not altered, downstream gene expression analyses were not undertaken.

Robust hypermethylation was demonstrated at hypomethylated cg21511203. CpG methylation downstream of the gRNA increased by 1.3%, 28.6% (cg21511203), 24.3%, and 25.8% respectively. This increase in methylation impacted the expression of *PARP10,* demonstrating a significant reduction, with no change in *PLEC* or *GRINA* (Figure 3G). Previously reported chromatin interaction data indicated that the regions harboring the CpG sites physically interact with *PLEC* in none-cartilaginous cell lines[11]. Further to this we subsequently confirmed chromatin interactions linking CpGs with the transcription start site of *PLEC* but not *PARP10* or *GRINA* in data from primary chondrocytes [39]. The combination of epigenetic modulation and chromatin interaction data therefore prioritised *PLEC* for downstream analyses.

**CRISPR-based editing of plectin in iASC-s9c9 is efficient at the DNA, mRNA, and protein level, and is maintained throughout chondrogenesis**

To explore the effect of plectin deficiency *in vitro*, the immortalised *SOX9* overexpression and inducible Cas9 containing adipose-derived chondrogenic cell line (iASC-s9c9) was used to generate a 26 bp deletion in exon 3 of *PLEC* using paired gRNA. Western blot for Cas9 induction is demonstrated in Figure S5. Inducible iASC-s9c9 was gene edited by transfecting gRNAs for 48 hr (Figure 4A). This resulted in a knockout that was less than 100% efficient at the DNA level, demonstrated by a PCR product with 3 bands of equivalent intensity in gene-edited cells (Figure 4B). Based on the gel electrophoresis, approximately one-third of

548 this DNA had a paired guide cut, with a deletion 26 bp smaller than the control amplicon size
549 of 293 bp. This middle band (293 bp) likely represents unedited DNA, or DNA containing
550 single-guide edits that cannot be resolved on the 3% gel used, a consequence of CRISPR/Cas9-
551 based edits using a single gRNA. The upper, higher molecular weight band was hypothesized
552 to be a heteroduplex formation of edited and CTRL bands. Therefore, the DNA edit was
553 interpreted to be at least two-thirds of the molecules representing the lower and upper bands,
554 with a proportion of single-guide edits in the CTRL band (figure 4B). Sanger sequencing of
555 the lower band confirmed a 26 bp deletion of the expected DNA sequence in exon 3 of *PLEC*
556 (Figure 4D and S6). Cell expansion followed by western blotting demonstrated >50% reduction
557 of plectin at early (P1) and late (P6) passages in monolayer (Figure 4E, full western blots Figure
558 S7). Despite being a sub-total knockout, as this line was generated with CRISPR deletion, it
559 was designated as iASC-s9c9-plectin-knockout (*PLEC*-KO) and was used in subsequent
560 experiments. No evidence of changes in DNA, mRNA, or protein was present in the CTRL
561 line (Figure 4B, E, F).

562 We next assessed the expression of *PLEC* throughout pellet chondrogenesis, detecting
563 an upregulation from d0 to d42 in CTRL pellets, with suppressed upregulation in *PLEC*-KO.
564 Relative *PLEC* mRNA expression remained 50% lower in *PLEC*-KO but increased
565 comparably to CTRL (Figure 4F). The level of plectin reduction in chondrocytes in pellets
566 after d42 days of culture was more pronounced than in monolayer, as *PLEC* expression failed
567 to increase even with chondrogenesis (Figure S7, 4F). In summary, *PLEC* is upregulated
568 throughout chondrogenesis, however Cas9-mediated deletion of exons of *PLEC* impacts
569 transcription and the translation of *PLEC* mRNA into plectin, which is more marked by the
570 end of chondrogenesis.
571

**Plectin deficiency in iASC-s9c9 chondrogenesis demonstrates transcriptomic changes in OA relevant pathways**

To determine the impact of plectin deficiency on cartilage development, we used two complementary 3D *in vitro* model systems of chondrogenesis. CTRL and *PLEC*-KO iASC-s9c9 lines were differentiated either as pellet cultures or encapsulated in an agarose hydrogel and chondrogenically differentiated for 42 days. For a phenotypic assessment of chondrogenesis, gene expression was assessed by comparing the fold change expression from d0 to d42 in pellets by qPCR or by comparative RNAseq of d42 agarose constructs seeded with CTRL or *PLEC*-KO cells. Matrix production using histological and IHC in both systems. This approach allowed a systematic assessment of the impact of plectin deficiency on cartilage formation across multiple models, where consistent trends across systems were more likely to be biologically meaningful.

qPCR demonstrated reduced expression of *PLEC* in pellets derived from *PLEC*-KO compared to CTRL (Figure 4F), however the difference in fold change (FC) upregulation from d0 to d42 between lines was non-significant (Figure 5A). As *SOX9* is a master regulator of chondrocyte anabolism, we assessed whether *PLEC*-KO impacted the expression of *SOX9* (Figure 5A). *SOX9* upregulation was significantly higher in *PLEC*-KO than in CTRL pellets between d0 and d42 ($P = 0.015$) (Figure 5A). However, molecular markers of anabolism, *ACAN* and *COL2A1,* showed a greater upregulation in CTRL pellets (Figure 5A). The expression of *ACAN, COL2A1, SOX9* and *PLEC* was not significantly different in d42 agarose constructs (data not shown).

*PLEC*-KO chondrocytes demonstrated a lower upregulation/expression of *COL1A1* and *COL10A1* in pellets and agarose constructs respectively, suggesting a degree of protection from fibrosis and hypertrophy (Figure 5A). Of note, in both systems overall *COL1A1* and *COL10A1* expression was much lower than anabolic gene expression, reflecting that iASC-

s9c9 chondrogenesis was globally less hypertrophic/fibrotic than anabolic (CTRL agarose constructs mean CPM; *COL10A1* = 64, *COL1A1* = 1684, *COL2A1* = 26142, *ACAN* = 30933). Next, the expression of catabolic genes *MMP13* and *ADAMTS5* was assessed. *MMP13* upregulation was significantly lower in *PLEC*-KO, while *ADAMTS5* was equivalent, indicating no clear catabolic phenotype associated with plectin deficiency (Figure 5A). Similarly to fibrotic/hypertrophic expression, catabolic gene expression was relatively low in agarose constructs, with *ADAMTS5* and *MMP13* being minimally expressed (both mean CPM <1).

At the matrix level, no detectable difference was demonstrated in Safranin-O staining (Figure 5C). Quantitatively, no significant difference in GAG/DNA was observed between *PLEC*-KO and CTRL in d21/42 pellet or agarose cultures (Figure 5B). Histological phenotypes were further assessed using IHC for type II and type X collagen, with no clear observable difference corresponding with the molecular phenotype. In summary, the significantly lower expression of *ACAN* and *COL2A1* in *PLEC-KO* pellets did not impact matrix production or GAG quantification.

**Plectin deficiency does not affect mechanical stiffness or calcium signalling**

The structural dynamics of the cytoskeleton have been linked to regulating calcium signalling [35, 36, 40, 41]. To assess whether plectin deficiency-associated alterations in matrix related signalling pathways and chondrocyte function affect calcium signalling, atomic force microscopy (AFM) was used. We aimed to characterize changes in chondrocyte morphological, mechanical and mechanoresponsive parameters in response to deformation. Measuring the height of CTRL and *PLEC*-KO chondrocytes revealed no significant difference (Figure 6A). We then assessed the extent of deformation of individual chondrocytes after loading at 500 nN and the subsequent relative calcium signalling in response to this load. Deformation (defined as percentage change in total cell height after load application) showed

no significant difference between the cell lines (Figure 6B). In line with these results, quantification of relative calcium signalling revealed no difference between *PLEC-KO* and CTRL (Figure 6C). Comparable responder rates of 22.4% (CTRL) and 18.4% (*PLEC*-KO) were obtained when calculating the percentage of cells that responded to the applied load with a calcium signalling response (Figure 6D).

**Effect of plectin deficiency on response to inflammation at the molecular and tissue level**

Inflammation is commonly a driver of OA development and progression, and affects cartilage after skeletal maturation[42], therefore, we assessed the impact of plectin deficiency on the response of engineered cartilage to inflammation *in vitro*, following the completion of chondrogenesis. For this, *PLEC*-KO and CTRL were exposed to 1 ng/ml of the cytokine IL-1β or left untreated to serve as a control. The expression of chondrogenic genes was used to assess for molecular phenotypes after inflammatory challenge. *SOX9* was significantly reduced in response to IL-1β in both lines, with no significant difference between lines (Figure 7A). *PLEC* demonstrated significant upregulation in response to IL-1β in both lines, with a trend towards reduced upregulation in *PLEC*-KO pellets, however this difference was not significant (Figure 7A). In response to inflammatory challenge, expression of *ACAN*, *COL2A1*, and *COL1A1* were significantly decreased, while *COL10A1* was significantly increased in both CTRL and *PLEC*-KO pellets (Figure 7A). The expression of inflammatory markers *ADAMTS5* and *MMP13* were significantly increased after IL-1β treatment (Figure 7B). Next, we assessed the expression of IL*6,* a well-recognized downstream marker of interleukin-1 signalling,[43] to determine changes in inflammatory signalling with plectin deficiency. Of note, our results show that plectin deficiency appeared to inhibit inflammatory signalling, which was reflected in reduced *IL6* upregulation in *PLEC-KO* (Figure 7B).

Given the changes in inflammatory signalling in plectin-deficient cells at the gene expression level, we next investigated the effect of IL-1β in matrix production using histological and quantitative biochemical analyses. Our results demonstrated significantly reduced GAG/DNA in pellets derived from both lines (Figure 7C). However, an interaction analysis showed the effect of plectin deficiency on this response was not significant (Figure 7C). This was reflected in Safranin O staining, which did not demonstrate an observable difference in the amount of GAG loss in *PLEC*-KO pellets compared to CTRL after IL-1β treatment (Figure 7F). Concordant with these findings, IHC demonstrated a reduction of type II collagen and modest increase of type X collagen in both CTRL and *PLEC*-KO chondrocytes after IL-1β treatment (Figure 7D, E). Overall, histology demonstrated clear effects of IL-1β on type II collagen, GAG and type X collagen. However, plectin deficiency did not appear to have a clear impact on the susceptibility of the ECM inflammation at the tissue level.

Next, AFM was used to measure the elastic modulus of chondrogenic pellets following inflammatory treatment (Figure 7G). Indentation analyses demonstrated no significant differences in pellet stiffness between untreated groups (Figure 8H), and in mechanical properties in response to inflammatory treatment (Figure 7H). In summary, both lines displayed an inflammatory response to IL-1β treatment, demonstrating significant interactions with between plectin deficiency and inflammatory signalling at the molecular level, that did not consistently translate to differences in matrix production or mechanical properties.

**Transcriptomic phenotyping of mechanical loading**

To assess the response to mechanical loading, pair-wise comparisons were made between unloaded, free-swelling (FS) controls and loaded constructs. The number of DEGs for each comparison in the immediate response to load were quantified (Figure 8A). Immediately after mechanical loading (Figure 8A), *PLEC*-KO had a greater number of overall DEGs

(CTRL: 806, *PLEC*-KO: 874). CTRL exhibited a lower number of upregulated and a larger number of downregulated DEGs than *PLEC*-KO constructs (CTRL: 415 up, 391 down, *PLEC*-KO: 595 up, 279 down) (Figure 8A). RNAseq data was then cross-referenced to assess the expression of previously validated load-responsive genes[29, 37]. The expression of prostaglandin-endoperoxide synthase-2 (*PTGS2*), Nuclear Factor of Activated T Cells 2 (*NFATC2*), Inhibin Subunit Beta A (*INHBA*), C-X-C Motif Chemokine Ligand 8 (*CXCL8*) and Bone Morphogenetic Protein 2 (*BMP2*) was assessed after exposing constructs to physiological levels of dynamic mechanical loading. In both cell lines, only *BMP2* and *NFATC2* were significantly upregulated in response to load, however, RNAseq data classified both genes as independent of plectin deficiency (KO-independent, KOI genes). The RNAseq DEG analysis platform (Figure S2) was applied to identify genes that were DEGs in response to load in *PLEC*-KO constructs but not in CTRL constructs, therefore, DEGs unique to plectin deficiency (KO-induced-response, KIR genes). In *PLEC*-KO, there were 457 unique KIR genes (301 upregulated, 156 downregulated). To further sub-stratify the KIR data into the most biologically relevant genes, the top 100 upregulated and downregulated genes were filtered with a CPM of 10 (mean expression across all loaded and unloaded samples) and sorted by fold change difference when compared to controls.

This approach identified the top 10 most significant genes with a relatively high expression value (CPM >10), and the largest relative fold change in response to load in *PLEC*-KO only. The top 3 upregulated KIR genes with reported functions were: Transgelin (*TAGLN*), lecithin-cholesterol acyltransferase (*LCAT*), and long non-coding (lnc) RNA *AC245100.4*. *TAGLN* is a *TGF-β* inducible gene that regulates osteoblastic and adipogenic differentiation of human skeletal stem cells through actin cytoskeleton organization[44], catalyzing the transfer of an unsaturated fatty acid from lecithin to free cholesterol, producing lysolecithin and cholesteryl ester[45]. In humans, *LCAT* deficiency results in an autosomal recessive inherited

disease that presents with corneal opacity, dyslipidemia and proteinuria[46]. *AC245100.4* promotes prostate cancer tumorigenesis via the microRNA-145-5p/RB binding protein 5, histone lysine methyltransferase complex subunit (*RBBP5*) axis. A clear function of lncRNA *AC138028.2* has not been previously described; however, it overlies exons of *PIEZO1* on chromosome 16, and therefore, could play a role in epigenetic regulation of *PIEZO1* expression.

The top 3 downregulated KIR genes with reported functions were: microsomal glutathione S-transferase 1 (*MGST1*), ectonucleotide pyrophosphatase/phosphodiesterase 2 (*ENPP2*), and ERI1 exoribonuclease family member 2 (*ERI2*). *MGST1* is expressed in high amounts in the liver; it encodes an enzyme that is activated by oxidative stress, with a localization in both the endoplasmic reticulum and the inner and outer mitochondrial membranes[47]. It has been reported that overexpression of *MGST1* induces gastric carcinoma cell proliferation by activating the *Akt/GSK-3β* signalling pathway [48], and in human osteoarthritic meniscus, mechanical overload can drive overexpression of *MGST1* [49]. *ENPP2* also known as autotaxin (*ATX*), encodes a gene that secretes an extracellular lipid mediator termed lysophosphatidic acid (*LPA*). *ATX-LPA* has been reported to be a key regulator of cartilage formation. Its signalling promotes S-phase entry and chondrocyte proliferation *in vitro* and *in vivo*, through β1-integrin translocation leading to fibronectin assembly and further ECM deposition, thereby promoting chondrocyte-matrix adhesion [50]. *ATX* expression is elevated in severely degenerated cartilage compared to less degenerated cartilage, and local delivery of an *ATX* inhibitor partially attenuates surgically induced OA in mice [51]. *ERI2* is a gene with a paucity of information about its function; its encoded protein is a member of the ER1 family of exoribonucleases, which over the course of evolution (*ERI1* specifically) have been recruited into a variety of conserved and species-specific regulatory small RNA pathways

720 that include endogenous small interfering RNAs and microRNAs[52]. The top 10 ranked KIR
721 genes in response to load are presented in Figure 8C.

722
723 **Transcriptomic phenotyping of the mechano-inflammatory model**

724 We aimed to replicate key components of the *in vivo* arthritic environment by
725 challenging constructs with concurrent inflammatory and mechanical cues, followed by the
726 application of RNAseq. This was termed the mechano-inflammatory model. CTRL and *PLEC*-
727 KO were subjected to 72 hr inflammatory challenge followed by dynamic compression at
728 physiological levels for 3 hr. Following RNAseq QC, the sample numbers for each condition
729 are reported in Supplementary Table 4. An identical bioinformatic approach was used to
730 determine KIR genes. In the mechano-inflammatory model, there were 432 KIR genes (220
731 upregulated, 212 downregulated). The top 3 upregulated KIR genes were: spectrin beta, non-
732 erythrocytic 5 (*SPTBN5*), Cbp/p300 interacting transactivator with Glu/Asp rich carboxy-
733 terminal domain 2 (*CITED2*) and eukaryotic translation initiation factor 4A1 (*EIF4A1*).
734 *SPTBN5* encodes a spectrin, a member of a family of cytoskeletal proteins interacting with
735 actin filaments, microtubules, and intermediate filaments, and connecting the cytoskeleton to
736 the plasma membrane[53, 54]. Additionally, plectin has been demonstrated to bind directly to
737 spectrin[55]. *CITED2* mediates the crosstalk between mechanical loading and interleukin-4
738 (*IL-4)* to promote chondroprotection by downregulating *MMP13* in the presence of
739 inflammation in mice[56]. *CITED2* also has a role as a negative regulator for hypoxia-inducible
740 factor (*HIF*)-1α through its competitive binding with *HIF-1α* to *CBP/p300*[57]. *EIF4A1*
741 encodes a component of the eIF4F complex, which includes eIF4E, eIF4G, and eIF4A, proteins
742 that are essential for mRNA translation initiation[58].

743 The top 3 downregulated KIR genes were: *COL1A1*, miRNA H19 imprinted maternally
744 expressed transcript (*H19*), and colony-stimulating factor 2 (*CSF2*). *COL1A1*, a marker of
745 fibrosis, has been described in detail previously in this report. *H19* encodes miRNA-H19,

whose expression has been reported to be heavily dependent on *SOX9* in healthy human chondrocytes[59]. *H19* gives rise to the mature *miRNA-675*, and *SOX9* positively regulates *COL2A1* in human articular chondrocytes via an *miRNA-675*-dependent mechanism[59]. *CSF2* (also known as granulocyte–macrophage colony-stimulating factor, *GM-CSF*) is a proinflammatory multifunctional cytokine. In rheumatoid arthritis, *GM-CSF* plays a key role through activation, differentiation, and survival of macrophages, dendritic cells, and neutrophils[60]. Mavrilimumab (a human monoclonal antibody targeting *GM-CSF* receptor-α) significantly lowered rheumatoid arthritis disease activity in a phase IIb randomized clinical trial[60]. The top 10 KIR genes in this model are presented in Figure 8D.

## Discussion

We have identified and replicated novel mQTLs associated with a previously described OA SNP (rs11780978), utilizing epigenetic modulation to link methylation with expression of previously described OA risk genes. Subsequently, we developed, validated and employed a highly chondrogenic CRISPR-based pipeline to replicate and study the effect of an OA risk allele (plectin deficiency), on the development, maturation, and homeostasis of human cartilage *in vitro*. The findings of this study support our hypothesis that epigenetic regulation of *PLEC* by rs11780978 plays an important role in chondrogenesis, chondrocyte phenotype, and cartilage homeostasis in response to mechanical loading and mechano-inflammatory challenge.

We present replication of rs11780978 mQTLs at cg19405177 and cg14598846 in cartilage, and novel replications of three previously reported array CpGs (cg07427475, cg02331830 and cg23299254[11]) as well as the discovery and replication of a novel CpG in a unique physical location (cg21511203) in human cartilage. This data expands upon the knowledge base of known OA mQTLs. Of note, the correlation between methylation and genotype at the risk allele appears to be variable across the two clusters, as previously demonstrated[11]. Using the TC28a2 inducible-dCas9-TET-1 cell line, we demonstrate that

771 reducing CpG methylation levels is reproducible, with a broad range of site-specific
772 demethylation values. It has previously been established across multiple tissues that the
773 rs11780978 OA risk allele is associated with higher methylation at cluster 1 and cg21511203,
774 and with lower methylation at cluster 2 [11, 13]. Consistent with the presence of a cg14598846
775 meQTL at *PLEC*, cg14598846 and cg23299254 behave as predicted in this model system.
776 Modulating methylation at these sites altered mainly *PLEC* and *GRINA* expression. Combined
777 with previous allelic expression analysis (AEI) data [11, 13], this prioritised these as GOI. Due
778 to the SNP location, CpG site functional effects, chromatin interaction data from none-
779 cartilaginous[11], as well as cartilage [39] tissue, and previous literature on *PLEC* function, it
780 was prioritized for further analyses. At 6 CpGs there was evidence of a link between
781 methylation and expression of GOI, suggesting a regulatory function of these (and adjacent)
782 sites.

783 Plectin is a large, complex cytoskeletal protein involved in mechanotransduction and
784 the mechanical response of the cell to load [61, 62]. It has been associated with OA in genetic
785 and epigenetic analyses[11, 13]. With the increasing awareness of the concepts of
786 mechanobiology and inflammation in OA[42], aberrant mechanotransduction is gaining
787 increased interest as a major contributor to OA, and plectin may serve as a critical, but
788 understudied, regulator of these phenomena [11, 13]. Plectin deficiency in humans causes
789 multiple diseases, the most common being epidermolysis bullosa simplex, a skin blistering
790 disease, combined with progressive muscular dystrophy (EBS-MD) [63]. EBS-MD severity
791 varies with muscular weakness, representing the most debilitating factor. EBS-MD and other
792 plectinopathies have not previously been associated with OA, potentially as most patients, due
793 to limited life expectancies, lack the time to develop primary OA. There is currently no access
794 to primary chondrocytes from patients with these conditions to allow the study of disease
795 pathology. Data from the human protein atlas has demonstrated that *PLEC* is most highly

796 expressed in skeletal muscle, skin, and the cerebral cortex (normalised transcript per million,
797 TPM, approximately >100, >85 and > 60 respectively) [64]. We previously reported high
798 expression of *PLEC* in human cartilage (mean CPM 145 in OA cartilage)[11].

799 Building on the epigenetic data, we have undertaken deep phenotyping of *PLEC* and
800 plectin to validate a proof-of-concept pipeline for testing OA risk genes in the development
801 and homeostasis of a highly chondrogenic cell-based system. This system can be used to
802 generate CRISPR-Cas9 based reproducible edits at the DNA/mRNA and protein level,
803 providing an *in vitro* model to phenocopy the effect of risk alleles, in this case, plectin
804 deficiency. The genome editing was maintained through cellular expansion and did not prevent
805 the cells from being able to undergo primary chondrogenesis. As such, with this approach, the
806 function of multiple GOI can be investigated individually, sequentially, or in multiplex
807 (simultaneous transfection with gRNAs targeting multiple GOI). The pipeline generated in this
808 study represents a platform to study cartilage development and homeostasis, and the
809 intersection of other OA risk genes with these processes.

810 OA is polygenic, and phenotypes from a single SNP are likely to be subtle, despite a
811 near-total knockout of a large, multifunctional protein, observed phenotypes were mainly at
812 the molecular level. In *PLEC*-KO chondrocytes in monolayer, protein was reduced 40-50%
813 compared to control. During chondrogenesis, the level of plectin deficiency became more
814 pronounced, due to the inability of *PLEC*-KO cells to upregulate plectin to the same extent as
815 control. If these findings translated to human development, it could be hypothesised that
816 patients with the rs11780978 risk allele may exhibit reduced plectin levels in articular cartilage
817 following cartilage development *in vivo*. This model may therefore phenocopy the effect of an
818 OA risk allele. Our data highlight the complexity of OA genetic risk, which poses challenges
819 for studying the disease using genome editing approaches [65].

820 Plectin deficiency demonstrated various molecular and cellular phenotypes, which may

821 partially explain the association between the risk allele and OA development. Principally, the
822 reduced upregulation of *COL2A1* and *ACAN* observed may suggest that plectin deficient
823 cartilage may have a less anabolic phenotype. Paradoxical to our hypothesis, we observed
824 reduced *COL10A1* expression in *PLEC*-KO pellets. To our knowledge, there is no link between
825 plectin and Type X Collagen deposition or *COL10A1* expression. Increased expression and
826 abundance of hypertrophic collagens have been reported in OA onset and progression[66]. A
827 similar, albeit less pronounced effect was observed for *COL1A1* expression. When considering
828 potential mechanistic links between plectin deficiency and cartilage development or
829 homeostasis, plectin knockout in iASCs has previously been demonstrated to reduce expression
830 of genes related to Wnt signalling pathways, which are crucial for cartilage formation[67].
831 Further, it has been reported that in skeletal muscle development, plectin binds to Dishevelled-
832 2 (*DVL2*) and forms a protein complex, activating canonical Wnt signalling[68, 69]. Thus,
833 investigating plectin linked *DVL2*-dependent mechanisms in cartilage may be of relevance to
834 future studies.

835 Due to previously reported data on the role of plectin as a crucial component of
836 intermediate filament functionality, including processes such as mechanotransduction [28, 62,
837 70, 71], we sought to mechanically phenotype plectin deficient and CTRL chondrocytes using
838 AFM and mechanical/mechano-inflammatory loading. Cell stiffness is dependent on the
839 overall structure of the cytoskeleton; is a fundamental measure of the extent a living cell resists
840 mechanical deformation and may influence mechanobiologic responses to external
841 stresses[61]. Plectin deficiency may therefore have been expected to reduce cell stiffness, given
842 evidence that the protein binds to intermediate filaments and anchors them at peripheral
843 junctions (such as hemidesmosomes[72] and focal adhesions[73-75]). We did not observe this
844 effect, however, these findings may not be directly comparable to our data, as most previous
845 studies assessed cells fully or partially adherent on tissue-culture plastic, whereas our AFM

846 measurements were performed prior to cell adherence to glass coverslips[76, 77]. Future
847 experiments may assess whether plectin-deficient cells exhibit increased stiffness at earlier
848 time-points than those evaluated in our study.

849 As inflammation is a key component of OA development and progression[42, 78, 79],
850 we phenotyped the response to this in our system. Our findings demonstrate that IL-1β
851 stimulation results in significant downregulation of *ACAN*, *COL2A1*, *COL1A1,* and *SOX9* in
852 chondrogenic pellets. These responses were translated to the histological level, with reduced
853 Safranin O staining for GAG and IHC for Type II Collagen. Plectin deficiency was associated
854 with less *IL6* upregulation when compared to controls but an equivalent suppression of *ACAN*
855 and *COL2A1*. These data may suggest the activation of alternative inflammatory signalling
856 pathways, or increased susceptibility to inflammation in plectin-deficient cells subjected to
857 inflammatory environments[36, 40, 80, 81].

858 In our aim to test our edited cells in OA mimetic conditions, we developed a model of
859 cell exposure to mechanical loading in the presence or absence of inflammation. After the
860 application of dynamic mechanical loading, the robust upregulation of previously described
861 load-responsive pathways [37] was identified. We also report novel gene targets that interact
862 with plectin deficiency in response to these stimuli. Our study identifies interactions between
863 loading, plectin deficiency and a lncRNA (*AC138028.2*) which has not been previously
864 described in chondrocyte biology. *AC138028.2* overlies exons of *PIEZO1* on chromosome 16
865 and therefore may warrant further study as a plectin-linked regulator of the *PIEZO1* dependent
866 load response in chondrocytes [36, 40, 80, 81]. Similarly, other potential targets for
867 downstream mechanistic studies were identified, including *TAGLN*, a *TGF-β*-inducible gene
868 which influences cytoskeleton organisation[44], and is more highly expressed in the deep zone
869 chondrocytes in bovine cartilage[82]. One of the most highly differentially downregulated KIR
870 genes in the absence of inflammation was *PCDHGA3*. It has been suggested that lower

expression of *PCDHGA3* is associated with poorer biological ageing and frailty scores[83]. Therefore plectin-dependent downregulation of *PCDHGA3* may be involved in unhealthy ageing of chondrocytes. There is currently a paucity of evidence for a role for this gene in musculoskeletal biology.

In the presence of inflammation, the knockout specific downregulation of *H19* may provide mechanistic insights linking plectin deficiency with the development and progression of OA, as *H19* has been reported as an attractive marker for chondrocyte anabolism[84]. *SOX9* positively regulates *COL2A1* in human articular chondrocytes via a *miRNA-675 (*derived from *H19*) dependent mechanism[59]. Therefore, in the arthritic joint, plectin deficiency-associated downregulation of *H19* may result in reduced anabolic (e.g. *COL2A1*) gene expression and ECM deposition in response to mechanical loading. This could contribute to inadequate *COL2A1* repair mechanisms in plectin-deficiency.

## Conclusion

We report a functional pipeline to test a non-coding OA SNP from epigenome editing, through genome editing and downstream deep phenotypic characterisation of genes of interest via *in vitro* cartilaginous model systems replicating the mechano-inflammatory environment. This system, combined with RNAseq, enabled us to identify multiple novel links between the functional region, plectin and chondrocyte biology. These data enhance our knowledge on plectin biology and provide new pathways of interest for future study.

## Figure legends

**Figure 1. Physical location and arrangement of rs11780978 and 12 associated mQTLs**. **(A)** Region of chromosome 8 demonstrating location of clusters 1 and 2, the association SNP, and two of the three novel mQTLs (cg24891660 is grouped with cluster 1 in panel B). Arrows represent 5' to 3' reading direction for *PLEC*, *PARP10* and *GRINA*. E2 = *PLEC* exon 2, E30 = *PLEC* exon 30 (2 additional downstream *PLEC* exons, exons 31 and 32, were not included in the schematic due to the size of the gene and to allow for full comparative visualization of *GRINA* and *PARP10*). All 8 alternatively spliced human *PLEC* first coding exons identified are demonstrated. The region shown covers from ~145,000,000-145,070,000, hg19 assembly, UCSC Genome Browser. **(B)** Zoomed version demonstrating location of original cluster 1 CpGs with addition of cg24891660, proximity to cluster 2, and the physical relationship between both clusters. **(C)** Distance between Cluster 2, association SNP rs11780978 and novel CpGs cg21511203 and cg07212837. Adapted from [11].

**Figure 2. rs11780978 mQTLs and methylation analysis of TC28a2 and iASC-s9 cell lines at each replicated CpG.** Association between rs11780978 genotype (G/G; homozygous for the none-risk allele, A/G; heterozygous for the risk allele, A/A; homozygous for the risk allele) and methylation of six mQTL CpGs in patient cartilage, TC28a2 (TC28, genotype A/G) and iASC-s9 (ASCS9, genotype GG) DNA. *P*-values were calculated using the Kruskal-Wallis test in reference to the patient samples only. Horizontal lines and error bars show the mean ± SEM. n = the number of patients providing data per CpG site. n = ≥ 3 for the cell line DNA.

**Figure 3. Epigenome modulation of all mQTL CpGs via TC28a2-dCas9-TET-1 (A-F) and dCas9-DNMT3a (G).** Left panel in each CpG. Pyrosequencing data shows a 20 bp gRNA directs the dCas9-TET-1 to the region, hypomethylating the target CpG and generally demethylating other CpGs captured on the assay, apart from cg21511203, which was hypomethylated initially. X-axis demonstrates the physical distance between gRNA, other CpGs on the assay, and location of the array CpG, with + and – denoting distance from array CpG in base pairs. Percentages demonstrate absolute reduction in methylation at each site. Points and error bars demonstrate the mean ± SEM for n = 6 replicates. Right panel in each CpG, qPCR analysis of GOI showing normalised fold change expression of each gene in control cDNA when compared to samples targeted with gRNA after confirmation of demethylation. n = 6 replicates, *P* values calculated with paired t-test. NS, not significant ($P > 0.05$). **(G)** Pyrosequencing data shows that a 20 bp gRNA directs the dCas9-DNMT3a to the region, methylating the target CpG and other CpGs captured on the assay. X-axis demonstrates physical distance between gRNA, other CpGs on the assay and location of the array CpG. Percentages represent absolute increase in methylation at each site. Points and error bars demonstrate the mean ± SEM for n = 6 replicates. **(B)** qPCR analysis of genes interest showing normalised fold change expression of each gene in control cDNA when compared to samples targeted with gRNA after confirmation of demethylation. *P* value calculated with paired t-test. NS, not significant ($P > 0.05$).

**Figure 4. Validation of iASC-s9c9, iASC-s9c9-CTRL and iASC-s9c9-*PLEC*-KO. (A)** Western blot demonstrating no Cas9 expression in control without doxycycline, with progressively increasing Cas9 protein expression 24 hr and 48 hr after induction with doxycycline (DOX). **(B)** flanking PCR 3% agarose gel electrophoresis of the 26 bp deletion

demonstrating 3 bands. Lower band representing paired guide edit, upper band hypothesised to be heteroduplex formation, middle band representing wild type 293 bp or single guide editing that cannot be resolved on the gel. **(C**) iASC-s9c9 d42 pellet stained with Safranin O demonstrates extensive GAG staining **(D)** Representative Sanger DNA sequencing traces of iASC-s9c9-pC (CTRL) and iASC-s9c9-*PLEC*-KO (*PLEC*-KO) demonstrating deletion of 26 bp sequence in exon 3 of *PLEC* at P1 post-editing. **(E**) Western blot for plectin demonstrating reduction at passage 1 (P1) post-editing, maintained and enhanced by P6 post-editing in iASC-s9c9. GAPDH loading control is used for both western blots. **F)** qPCR mRNA quantification demonstrates significantly lower relative *PLEC* expression in CTRL vs *PLEC*-KO, which becomes more evident as *PLEC* upregulation in late chondrogenesis is inhibited by the edit. Unpaired t-test comparison within each time point, n = 6-9 pellets.

**Figure 5. Summary of gene expression, histological and immunohistochemical phenotypes of plectin deficiency in pellet and agarose culture. (A)** Fold change expression from d0 to d42 of *PLEC,* markers of anabolic (*SOX9, ACAN*, and *COL2A1*), hypertrophic (*COL10A1),* fibrotic (*COL1A1)* and catabolic *(ADAMTS5/MMP13)* signalling (n = 6-9 pellets/condition). No significant difference in matrix deposition between CTRL and *PLEC*-KO pellets and agarose constructs, as assessed (**B**) quantitatively by GAG/DNA in d21 and 42 pellets and d42 agarose constructs (n = 10-11, n = 11-14, n = 6-9 and n = 10-11 respectively), and **(C**) Qualitatively as shown by representative histological staining for GAG by Safranin O staining, and Type II and Type X Collagen by IHC (n ≥ 3 pellets.) Mean ± SEM. Statistics, unpaired t-test between groups.

**Figure 6. iASC-s9c9-derived chondrocytes mechanical properties are comparable regardless of plectin deficiency.** AFM measurements reveal no significant difference in **(A)** chondrocyte height **(B)** deformation (mean ± SEM). **(C)** calcium signalling intensity between CTRL and *PLEC*-KO. % represents overall percentage of responders (n = 116 CTRL vs n = 106 *PLEC*-KO) in each group Each datapoint represents one cell loaded by AFM. Solid and dashed horizontal lines represent inter-quartile range and median, respectively; Statistics assessed using unpaired t-test for each comparison. ns = not significant.

**Figure 7. Response of plectin deficient iASC-s9c9-derived pellets to inflammation.** **(A)** Gene expression of anabolic, fibrotic, and hypertrophic markers following inflammatory challenge demonstrates no significant interaction between CTRL and *PLEC*-KO. **(B)** inflammatory gene expression following IL-1β treatment in both lines, with *IL6* demonstrating a significantly higher upregulation in CTRL **(C)** GAG/DNA showing a significant reduction after inflammatory stimulus with no significant interaction. n = 6 pellets/line/treatment **(D-F)** Representative Safranin O staining for GAG and IHC for type II and type X collagen demonstrating reduced matrix deposition in CTRL and *PLEC*-KO pellets treated with IL-1β, but no effect of plectin editing **(G)** Representative AFM imaging of indentation of untreated cartilage pellet **(H)** AFM indentation demonstrates no difference in the mechanical properties with *PLEC*-KO. N = 2-4 cryosections/pellet, n = 2-3 pellets/line/treatment. Mean ± SEM. Statistics assessed using 2way ANOVA with Šidák correction, p value reported for effect of line. ns, not significant, $P > 0.05$, * $P = \leq 0.05$, ** $P = \leq 0.01$, *** $P = \leq 0.001$, **** = $P \leq 0.0001$.

**Figure 8. DEGs and KO-induced-response (KIR) genes after mechanical loading and in a mechano-inflammatory environment (A)** Quantification of DEGs demonstrates that *PLEC*-KO constructs have a greater number of upregulated and downregulated DEGs in

response to load, as well as mechanoinflammation compared to CTRL. **(B)** Significant upregulation of *NFATC2* and *BMP2* after loading, with no difference associated with plectin deficiency. (N= 3-5 constructs). Mean ± SEM. Statistical significance represents pAdj from RNAseq **** $P = \leq 0.0001$. r = gene rank (by pAdj) in response to load in each cell line compared to not loaded controls **(C)** green, upregulated and red, downregulated KIR genes. Genes were initially sorted by pKO 2 vs 1 (loaded vs not loaded) and pAdj to identify the top 100 most significant genes in each direction. A gene expression filter (mean counts per million, CPM, across all pKO/pC) of >10 was applied to identify the most biologically relevant genes by expression in agarose constructs. The top 100 genes were then ranked by relative Log2FC (L2FC) in pKO 2 vs 1 when compared to pC 2 vs 1, this provided a list of the genes with the highest pAdj, relatively high expression in cartilage and the highest differential fold change in pKO vs pC. **(D)** the identical approach was applied to identify KIR genes within the mechano-inflammatory.

## References


1. O'Neill TW, McCabe PS, McBeth J: **Update on the epidemiology, risk factors and disease outcomes of osteoarthritis**. *Best Pract Res Clin Rheumatol* 2018, **32**(2):312-326.
2. Goldring MB, Otero M: **Inflammation in osteoarthritis**. *Curr Opin Rheumatol* 2011, **23**(5):471-478.
3. Zhang Y, Jordan JM: **Epidemiology of osteoarthritis**. *Rheum Dis Clin North Am* 2008, **34**(3):515-529.
4. Silverwood V, Blagojevic-Bucknall M, Jinks C, Jordan JL, Protheroe J, Jordan KP: **Current evidence on risk factors for knee osteoarthritis in older adults: a systematic review and meta-analysis**. *Osteoarthritis Cartilage* 2015, **23**(4):507-515.
5. Runhaar J, van Middelkoop M, Reijman M, Vroegindeweij D, Oei EH, Bierma-Zeinstra SM: **Malalignment: a possible target for prevention of incident knee osteoarthritis in overweight and obese women**. *Rheumatology (Oxford)* 2014, **53**(9):1618-1624.
6. Saberi Hosnijeh F, Zuiderwijk ME, Versteeg M, Smeele HT, Hofman A, Uitterlinden AG, Agricola R, Oei EH, Waarsing JH, Bierma-Zeinstra SM *et al*: **Cam Deformity and Acetabular Dysplasia as Risk Factors for Hip Osteoarthritis**. *Arthritis Rheumatol* 2017, **69**(1):86-93.
7. Gala L, Clohisy JC, Beaule PE: **Hip Dysplasia in the Young Adult**. *J Bone Joint Surg Am* 2016, **98**(1):63-73.
8. Loughlin J: **Genetic contribution to osteoarthritis development: current state of evidence**. *Curr Opin Rheumatol* 2015, **27**(3):284-288.
9. Aubourg G, Rice SJ, Bruce-Wootton P, Loughlin J: **Genetics of osteoarthritis**. *Osteoarthritis Cartilage* 2021.
10. Miranda-Duarte A: **DNA Methylation in Osteoarthritis: Current Status and Therapeutic Implications**. *Open Rheumatol J* 2018, **12**:37-49.
11. Rice SJ, Tselepi M, Sorial AK, Aubourg G, Shepherd C, Almarza D, Skelton AJ, Pangou I, Deehan D, Reynard LN *et al*: **Prioritization of PLEC and GRINA as Osteoarthritis Risk Genes Through the Identification and Characterization of Novel Methylation Quantitative Trait Loci**. *Arthritis Rheumatol* 2019, **71**(8):1285-1296.
12. Parker E, Hofer IMJ, Rice SJ, Earl L, Anjum SA, Deehan DJ, Loughlin J: **Multi-Tissue Epigenetic and Gene Expression Analysis Combined With Epigenome Modulation Identifies RWDD2B as a Target of Osteoarthritis Susceptibility**. *Arthritis Rheumatol* 2020.
13. Sorial AK, Hofer IMJ, Tselepi M, Cheung K, Parker E, Deehan DJ, Rice SJ, Loughlin J: **Multi-tissue epigenetic analysis of the osteoarthritis susceptibility locus mapping to the plectin gene PLEC**. *Osteoarthritis Cartilage* 2020, **28**(11):1448-1458.
14. Rice SJ, Aubourg G, Sorial AK, Almarza D, Tselepi M, Deehan DJ, Reynard LN, Loughlin J: **Identification of a novel, methylation-dependent, RUNX2 regulatory region associated with osteoarthritis risk**. *Hum Mol Genet* 2018, **27**(19):3464-3474.
15. Kehayova YS, Watson E, Wilkinson JM, Loughlin J, Rice SJ: **Genetic and epigenetic interplay regulates COLGALT2, contributing to osteoarthritis genetic risk**. *Arthritis Rheumatol* 2021.
16. Shepherd C, Zhu D, Skelton AJ, Combe J, Threadgold H, Zhu L, Vincent TL, Stuart P, Reynard LN, Loughlin J: **Functional Characterization of the Osteoarthritis**

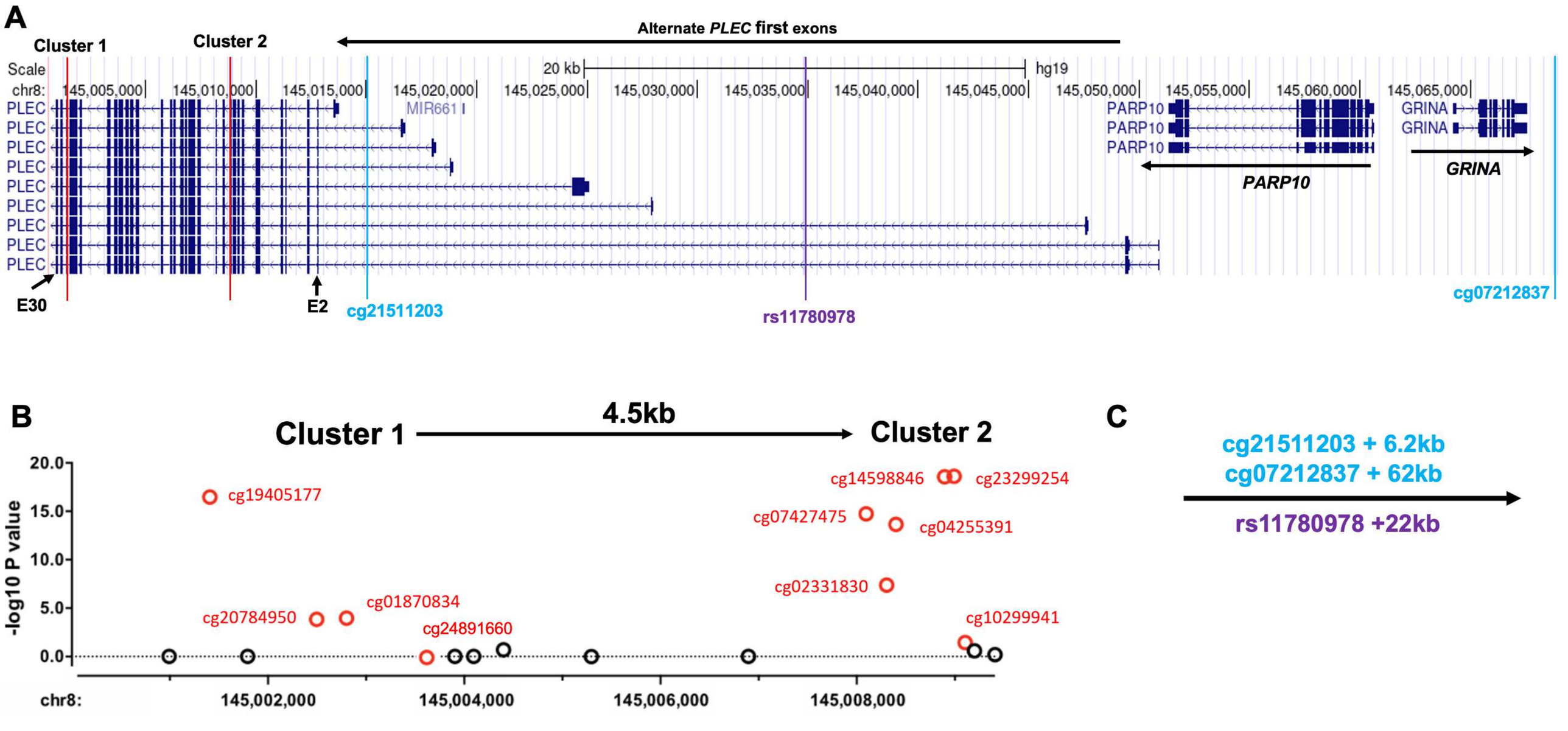
**Genetic Risk Residing at ALDH1A2 Identifies rs12915901 as a Key Target Variant**. *Arthritis Rheumatol* 2018, **70**(10):1577-1587.
17. Shepherd C, Reese AE, Reynard LN, Loughlin J: **Expression analysis of the osteoarthritis genetic susceptibility mapping to the matrix Gla protein gene MGP**. *Arthritis Res Ther* 2019, **21**(1):149.
18. Rice SJ, Cheung K, Reynard LN, Loughlin J: **Discovery and analysis of methylation quantitative trait loci (mQTLs) mapping to novel osteoarthritis genetic risk signals**. *Osteoarthritis Cartilage* 2019, **27**(10):1545-1556.
19. Rice SJ, Brumwell A, Falk J, Kehayova YS, Casement J, Parker E, Hofer IMJ, Shepherd C, Loughlin J: **Genetic risk of osteoarthritis operates during human skeletogenesis**. *Hum Mol Genet* 2022.
20. Loeser RF, Goldring SR, Scanzello CR, Goldring MB: **Osteoarthritis: a disease of the joint as an organ**. *Arthritis Rheum* 2012, **64**(6):1697-1707.
21. Collins KH, Haugen IK, Neogi T, Guilak F: **Osteoarthritis as a systemic disease**. *Nat Rev Rheumatol* 2026, **22**(2):105-117.
22. Buckwalter JA, Mankin HJ: **Articular cartilage: tissue design and chondrocyte-matrix interactions**. *Instr Course Lect* 1998, **47**:477-486.
23. Buckwalter J, Mankin H: **Articular cartilage: part I**. *Journal of Bone and joint surgery* 1997, **79**(4):600.
24. Huynh NP, Gloss CC, Lorentz J, Tang R, Brunger JM, McAlinden A, Zhang B, Guilak F: **Long non-coding RNA GRASLND enhances chondrogenesis via suppression of the interferon type II signaling pathway**. *Elife* 2020, **9**.
25. Huynh NPT, Zhang B, Guilak F: **High-depth transcriptomic profiling reveals the temporal gene signature of human mesenchymal stem cells during chondrogenesis**. *FASEB J* 2019, **33**(1):358-372.
26. Adkar SS, Wu CL, Willard VP, Dicks A, Ettyreddy A, Steward N, Bhutani N, Gersbach CA, Guilak F: **Step-Wise Chondrogenesis of Human Induced Pluripotent Stem Cells and Purification Via a Reporter Allele Generated by CRISPR-Cas9 Genome Editing**. *Stem Cells* 2019, **37**(1):65-76.
27. Zengini E, Hatzikotoulas K, Tachmazidou I, Steinberg J, Hartwig FP, Southam L, Hackinger S, Boer CG, Styrkarsdottir U, Gilly A *et al*: **Genome-wide analyses using UK Biobank data provide insights into the genetic architecture of osteoarthritis**. *Nat Genet* 2018, **50**(4):549-558.
28. Wiche G: **Plectin-Mediated Intermediate Filament Functions: Why Isoforms Matter**. *Cells* 2021, **10**(8).
29. Katz DB, Huynh NPT, Savadipour A, Palte I, Guilak F: **An immortalized human adipose-derived stem cell line with highly enhanced chondrogenic properties**. *Biochem Biophys Res Commun* 2020, **530**(1):252-258.
30. Barter MJ, Bui C, Cheung K, Falk J, Gomez R, Skelton AJ, Elliott HR, Reynard LN, Young DA: **DNA hypomethylation during MSC chondrogenesis occurs predominantly at enhancer regions**. *Sci Rep* 2020, **10**(1):1169.
31. Finger F, Schorle C, Zien A, Gebhard P, Goldring MB, Aigner T: **Molecular phenotyping of human chondrocyte cell lines T/C-28a2, T/C-28a4, and C-28/I2**. *Arthritis Rheum* 2003, **48**(12):3395-3403.
32. Goldring MB, Birkhead JR, Suen LF, Yamin R, Mizuno S, Glowacki J, Arbiser JL, Apperley JF: **Interleukin-1 beta-modulated gene expression in immortalized human chondrocytes**. *J Clin Invest* 1994, **94**(6):2307-2316.
33. Ran FA, Hsu PD, Wright J, Agarwala V, Scott DA, Zhang F: **Genome engineering using the CRISPR-Cas9 system**. *Nat Protoc* 2013, **8**(11):2281-2308.

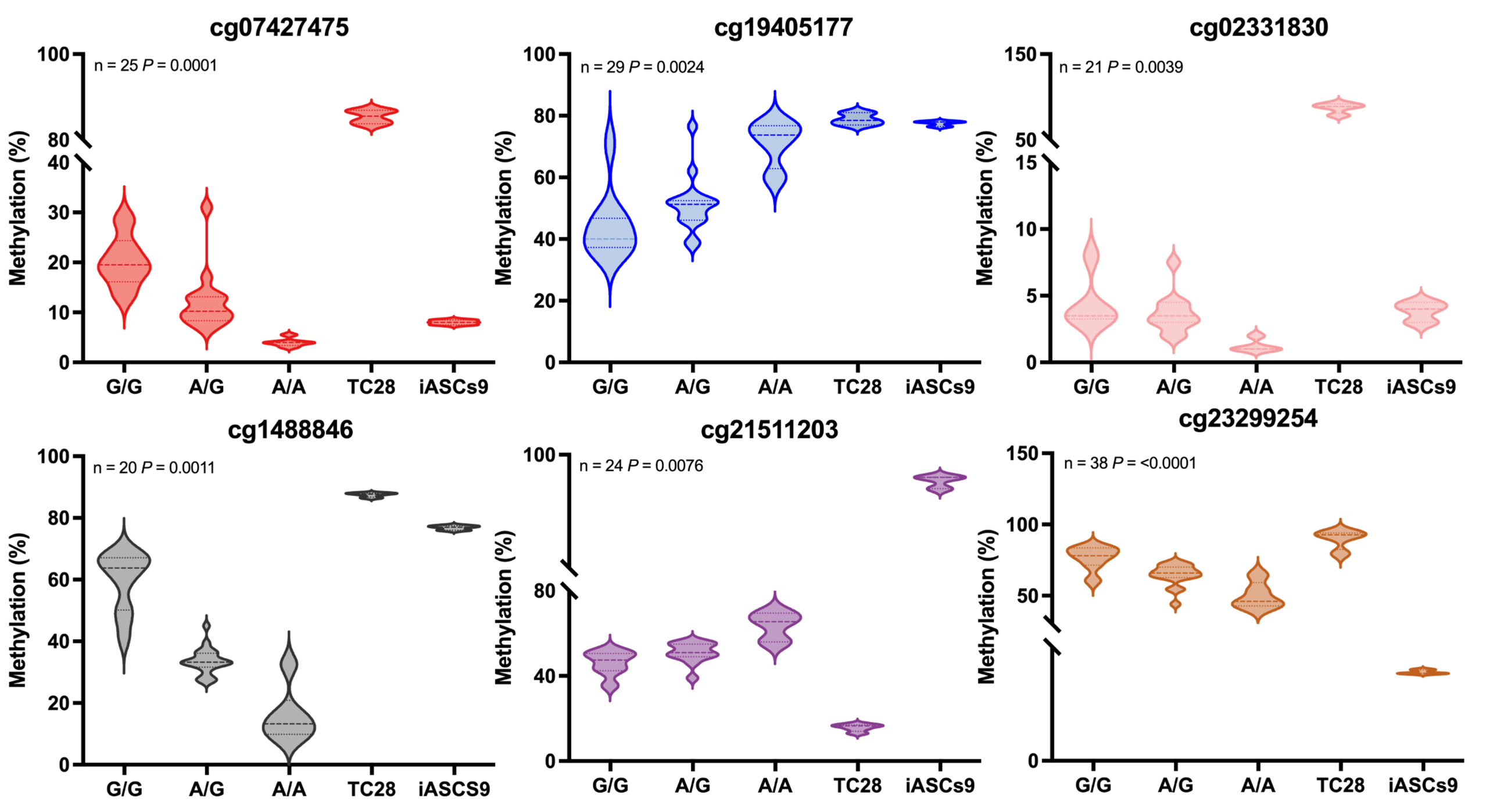
34. Wu CL, Dicks A, Steward N, Tang R, Katz DB, Choi YR, Guilak F: **Single cell transcriptomic analysis of human pluripotent stem cell chondrogenesis**. *Nat Commun* 2021, **12**(1):362.
35. Dicks AR, Maksaev GI, Harissa Z, Savadipour A, Tang R, Steward N, Liedtke W, Nichols CG, Wu CL, Guilak F: **Skeletal dysplasia-causing TRPV4 mutations suppress the hypertrophic differentiation of human iPSC-derived chondrocytes**. *Elife* 2023, **12**.
36. Savadipour A, Nims RJ, Rashidi N, Garcia-Castorena JM, Tang R, Marushack GK, Oswald SJ, Liedtke WB, Guilak F: **Membrane stretch as the mechanism of activation of PIEZO1 ion channels in chondrocytes**. *Proc Natl Acad Sci U S A* 2023, **120**(30):e2221958120.
37. Nims RJ, Pferdehirt L, Ho NB, Savadipour A, Lorentz J, Sohi S, Kassab J, Ross AK, O'Conor CJ, Liedtke WB *et al*: **A synthetic mechanogenetic gene circuit for autonomous drug delivery in engineered tissues**. *Sci Adv* 2021, **7**(5).
38. O'Conor CJ, Leddy HA, Benefield HC, Liedtke WB, Guilak F: **TRPV4-mediated mechanotransduction regulates the metabolic response of chondrocytes to dynamic loading**. *Proc Natl Acad Sci U S A* 2014, **111**(4):1316-1321.
39. Bittner N, Shi C, Zhao D, Ding J, Southam L, Swift D, Kreitmaier P, Tutino M, Stergiou O, Cheung JTS *et al*: **Primary osteoarthritis chondrocyte map of chromatin conformation reveals novel candidate effector genes**. *Ann Rheum Dis* 2024, **83**(8):1048-1059.
40. Lee W, Nims RJ, Savadipour A, Zhang Q, Leddy HA, Liu F, McNulty AL, Chen Y, Guilak F, Liedtke WB: **Inflammatory signaling sensitizes Piezo1 mechanotransduction in articular chondrocytes as a pathogenic feed-forward mechanism in osteoarthritis**. *Proc Natl Acad Sci U S A* 2021, **118**(13).
41. Lee W, Leddy HA, Chen Y, Lee SH, Zelenski NA, McNulty AL, Wu J, Beicker KN, Coles J, Zauscher S *et al*: **Synergy between Piezo1 and Piezo2 channels confers high-strain mechanosensitivity to articular cartilage**. *Proc Natl Acad Sci U S A* 2014, **111**(47):E5114-5122.
42. Vincent TL: **Mechanoflammation in osteoarthritis pathogenesis**. *Semin Arthritis Rheum* 2019, **49**(3S):S36-S38.
43. Cahill CM, Rogers JT: **Interleukin (IL) 1beta induction of IL-6 is mediated by a novel phosphatidylinositol 3-kinase-dependent AKT/IkappaB kinase alpha pathway targeting activator protein-1**. *J Biol Chem* 2008, **283**(38):25900-25912.
44. Elsafadi M, Manikandan M, Dawud RA, Alajez NM, Hamam R, Alfayez M, Kassem M, Aldahmash A, Mahmood A: **Transgelin is a TGFbeta-inducible gene that regulates osteoblastic and adipogenic differentiation of human skeletal stem cells through actin cytoskeleston organization**. *Cell Death Dis* 2016, **7**(8):e2321.
45. Mehta R, Elias-Lopez D, Martagon AJ, Perez-Mendez OA, Sanchez MLO, Segura Y, Tusie MT, Aguilar-Salinas CA: **LCAT deficiency: a systematic review with the clinical and genetic description of Mexican kindred**. *Lipids Health Dis* 2021, **20**(1):70.
46. Althaf MM, Almana H, Abdelfadiel A, Amer SM, Al-Hussain TO: **Familial lecithin-cholesterol acyltransferase (LCAT) deficiency; a differential of proteinuria**. *J Nephropathol* 2015, **4**(1):25-28.
47. Schaffert CS: **Role of MGST1 in reactive intermediate-induced injury**. *World J Gastroenterol* 2011, **17**(20):2552-2557.
48. Peng Z, Peng N: **Microsomal glutathione S-transferase 1 targets the autophagy signaling pathway to suppress ferroptosis in gastric carcinoma cells**. *Hum Exp Toxicol* 2023, **42**:9603271231172915.

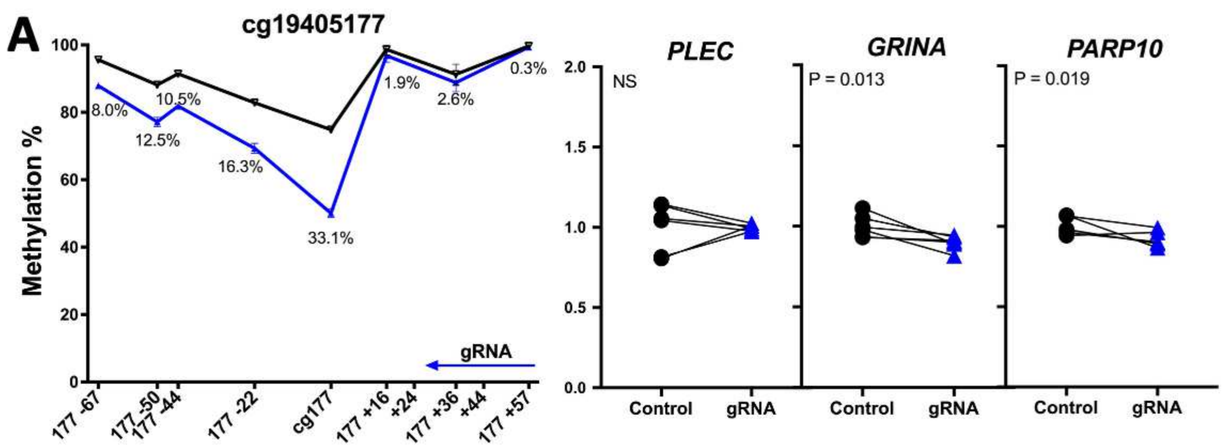
49. Wu X, Hamzatova A, Aulin C, Sun W, Struglics A, Hart DA, Ackermann PW, Ahmed AS: **Network Analysis Identifies Microsomal Glutathione S-Transferase as a Potential Regulator of Oxidative Stress and Proteasome Dysfunction in Human Osteoarthritic Menisci**. *FASEB Bioadv* 2026, **8**:e70101.
50. Nishioka T, Arima N, Kano K, Hama K, Itai E, Yukiura H, Kise R, Inoue A, Kim SH, Solnica-Krezel L *et al*: **ATX-LPA1 axis contributes to proliferation of chondrocytes by regulating fibronectin assembly leading to proper cartilage formation**. *Sci Rep* 2016, **6**:23433.
51. Datta P, Gandhi R, Nakamura S, Lively S, Rossomacha E, Potla P, Shestopaloff K, Endisha H, Pastrello C, Jurisica I *et al*: **Effect of autotaxin inhibition in a surgically-induced mouse model of osteoarthritis**. *Osteoarthr Cartil Open* 2020, **2**(3):100080.
52. Thomas MF, L'Etoile ND, Ansel KM: **Eri1: a conserved enzyme at the crossroads of multiple RNA-processing pathways**. *Trends Genet* 2014, **30**(7):298-307.
53. Khan A, Bruno LP, Alomar F, Umair M, Pinto AM, Khan AA, Khan A, Saima, Fabbiani A, Zguro K *et al*: **SPTBN5, Encoding the betaV-Spectrin Protein, Leads to a Syndrome of Intellectual Disability, Developmental Delay, and Seizures**. *Front Mol Neurosci* 2022, **15**:877258.
54. Rosenfeld JA, Xiao R, Bekheirnia MR, Kanani F, Parker MJ, Koenig MK, van Haeringen A, Ruivenkamp C, Rosmaninho-Salgado J, Almeida PM *et al*: **Heterozygous variants in SPTBN1 cause intellectual disability and autism**. *Am J Med Genet A* 2021, **185**(7):2037-2045.
55. Herrmann H, Wiche G: **Plectin and IFAP-300K are homologous proteins binding to microtubule-associated proteins 1 and 2 and to the 240-kilodalton subunit of spectrin**. *J Biol Chem* 1987, **262**(3):1320-1325.
56. He Z, Leong DJ, Xu L, Hardin JA, Majeska RJ, Schaffler MB, Thi MM, Yang L, Goldring MB, Cobelli NJ *et al*: **CITED2 mediates the cross-talk between mechanical loading and IL-4 to promote chondroprotection**. *Ann N Y Acad Sci* 2019, **1442**(1):128-137.
57. Yin Z, Haynie J, Yang X, Han B, Kiatchoosakun S, Restivo J, Yuan S, Prabhakar NR, Herrup K, Conlon RA *et al*: **The essential role of Cited2, a negative regulator for HIF-1alpha, in heart development and neurulation**. *Proc Natl Acad Sci U S A* 2002, **99**(16):10488-10493.
58. Steinmann SM, Sanchez-Martin A, Tanzer E, Cigliano A, Pes GM, Simile MM, Desaubry L, Marin JJG, Evert M, Calvisi DF: **eIF4A1 Is a Prognostic Marker and Actionable Target in Human Hepatocellular Carcinoma**. *Int J Mol Sci* 2023, **24**(3).
59. Dudek KA, Lafont JE, Martinez-Sanchez A, Murphy CL: **Type II collagen expression is regulated by tissue-specific miR-675 in human articular chondrocytes**. *J Biol Chem* 2010, **285**(32):24381-24387.
60. Burmester GR, McInnes IB, Kremer J, Miranda P, Korkosz M, Vencovsky J, Rubbert-Roth A, Mysler E, Sleeman MA, Godwood A *et al*: **A randomised phase IIb study of mavrilimumab, a novel GM-CSF receptor alpha monoclonal antibody, in the treatment of rheumatoid arthritis**. *Ann Rheum Dis* 2017, **76**(6):1020-1030.
61. Na S, Chowdhury F, Tay B, Ouyang M, Gregor M, Wang Y, Wiche G, Wang N: **Plectin contributes to mechanical properties of living cells**. *Am J Physiol Cell Physiol* 2009, **296**(4):C868-877.

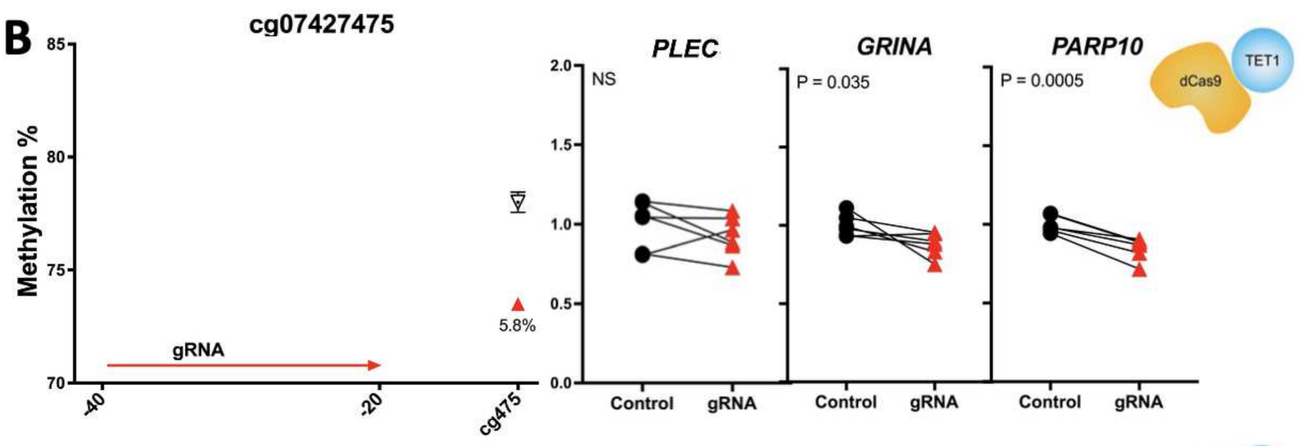
62. Almeida FV, Walko G, McMillan JR, McGrath JA, Wiche G, Barber AH, Connelly JT: **The cytolinker plectin regulates nuclear mechanotransduction in keratinocytes**. *J Cell Sci* 2015, **128**(24):4475-4486.
63. Winter L, Wiche G: **The many faces of plectin and plectinopathies: pathology and mechanisms**. *Acta Neuropathol* 2013, **125**(1):77-93.
64. Castanon MJ, Wiche G: **Identifying Plectin Isoform Functions through Animal Models**. *Cells* 2021, **10**(9).
65. Nowak MA, Boerlijst MC, Cooke J, Smith JM: **Evolution of genetic redundancy**. *Nature* 1997, **388**(6638):167-171.
66. Zhong L, Huang X, Karperien M, Post JN: **Correlation between Gene Expression and Osteoarthritis Progression in Human**. *Int J Mol Sci* 2016, **17**(7).
67. Usami Y, Gunawardena AT, Iwamoto M, Enomoto-Iwamoto M: **Wnt signaling in cartilage development and diseases: lessons from animal studies**. *Lab Invest* 2016, **96**(2):186-196.
68. Sharma M, Castro-Piedras I, Simmons GE, Jr., Pruitt K: **Dishevelled: A masterful conductor of complex Wnt signals**. *Cell Signal* 2018, **47**:52-64.
69. Yin H, Han S, Cui C, Wang Y, Li D, Zhu Q: **Plectin regulates Wnt signaling mediated-skeletal muscle development by interacting with Dishevelled-2 and antagonizing autophagy**. *Gene* 2021, **783**:145562.
70. Wiche G, Osmanagic-Myers S, Castanon MJ: **Networking and anchoring through plectin: a key to IF functionality and mechanotransduction**. *Curr Opin Cell Biol* 2015, **32**:21-29.
71. Staszewska I, Fischer I, Wiche G: **Plectin isoform 1-dependent nuclear docking of desmin networks affects myonuclear architecture and expression of mechanotransducers**. *Hum Mol Genet* 2015, **24**(25):7373-7389.
72. Rezniczek GA, de Pereda JM, Reipert S, Wiche G: **Linking integrin alpha6beta4-based cell adhesion to the intermediate filament cytoskeleton: direct interaction between the beta4 subunit and plectin at multiple molecular sites**. *J Cell Biol* 1998, **141**(1):209-225.
73. Seifert GJ, Lawson D, Wiche G: **Immunolocalization of the intermediate filament-associated protein plectin at focal contacts and actin stress fibers**. *Eur J Cell Biol* 1992, **59**(1):138-147.
74. Gonzales M, Weksler B, Tsuruta D, Goldman RD, Yoon KJ, Hopkinson SB, Flitney FW, Jones JC: **Structure and function of a vimentin-associated matrix adhesion in endothelial cells**. *Mol Biol Cell* 2001, **12**(1):85-100.
75. Bershadsky AD, Tint IS, Svitkina TM: **Association of intermediate filaments with vinculin-containing adhesion plaques of fibroblasts**. *Cell Motil Cytoskeleton* 1987, **8**(3):274-283.
76. Andra K, Nikolic B, Stocher M, Drenckhahn D, Wiche G: **Not just scaffolding: plectin regulates actin dynamics in cultured cells**. *Genes Dev* 1998, **12**(21):3442-3451.
77. Marks PC, Hewitt BR, Baird MA, Wiche G, Petrie RJ: **Plectin linkages are mechanosensitive and required for the nuclear piston mechanism of three-dimensional cell migration**. *Mol Biol Cell* 2022, **33**(12):ar104.
78. Zhou S, Maleitzke T, Geissler S, Hildebrandt A, Fleckenstein FN, Niemann M, Fischer H, Perka C, Duda GN, Winkler T: **Source and hub of inflammation: The infrapatellar fat pad and its interactions with articular tissues during knee osteoarthritis**. *J Orthop Res* 2022, **40**(7):1492-1504.

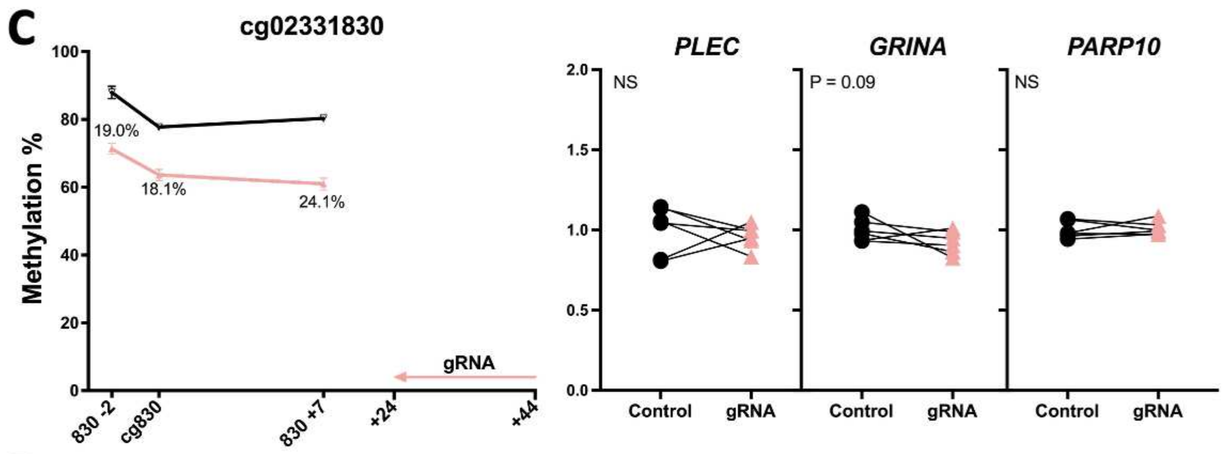
79. Cheng J, Li M, Bai R: **The Wnt signaling cascade in the pathogenesis of osteoarthritis and related promising treatment strategies**. *Front Physiol* 2022, **13**:954454.
80. Qin L, He T, Chen S, Yang D, Yi W, Cao H, Xiao G: **Roles of mechanosensitive channel Piezo1/2 proteins in skeleton and other tissues**. *Bone Res* 2021, **9**(1):44.
81. Lee W, Guilak F, Liedtke W: **Role of Piezo Channels in Joint Health and Injury**. *Curr Top Membr* 2017, **79**:263-273.
82. Delve E, Co V, Kandel RA: **Superficial and deep zone articular chondrocytes exhibit differences in actin polymerization status and actin-associated molecules in vitro**. *Osteoarthr Cartil Open* 2020, **2**(3):100071.
83. Kim S, Wyckoff J, Morris AT, Succop A, Avery A, Duncan GE, Jazwinski SM: **DNA methylation associated with healthy aging of elderly twins**. *Geroscience* 2018, **40**(5-6):469-484.
84. Steck E, Boeuf S, Gabler J, Werth N, Schnatzer P, Diederichs S, Richter W: **Regulation of H19 and its encoded microRNA-675 in osteoarthritis and under anabolic and catabolic in vitro conditions**. *J Mol Med (Berl)* 2012, **90**(10):1185-1195.

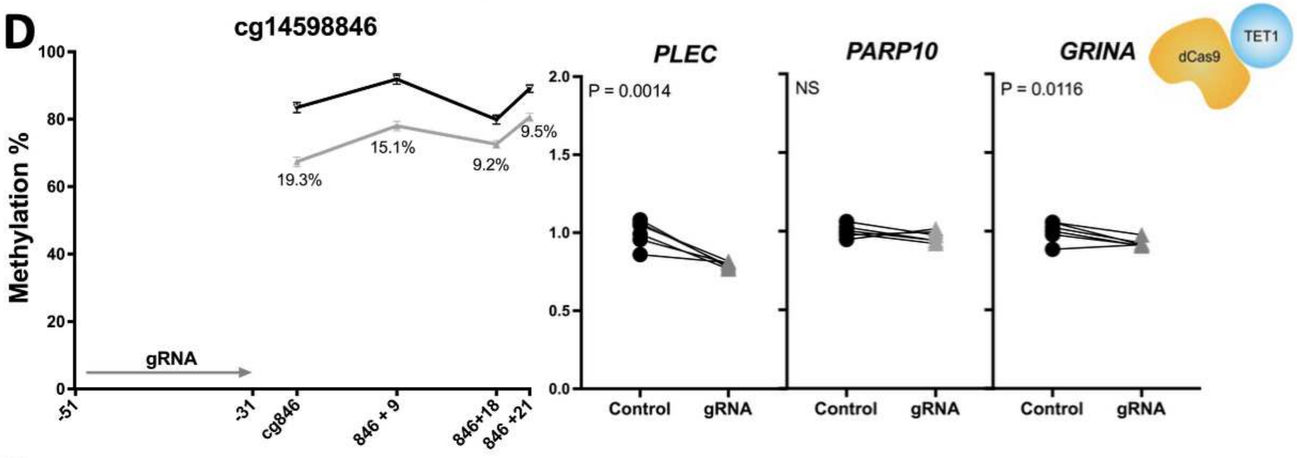

A
Cluster 1
Cluster 2
Alternate PLEC first exons
Scale
chr8:
20 kb
hg19
145,005,000
145,010,000
145,015,000
145,020,000
145,025,000
145,030,000
145,035,000
145,040,000
145,045,000
145,050,000
145,055,000
145,060,000
145,065,000
PLEC
MIR661
PARP10
GRINA
PARP10
GRINA
E30
E2
cg21511203
rs11780978
cg07212837
B
Cluster 1
4.5kb
Cluster 2
-log10 P value
20.0
15.0
10.0
5.0
0.0
cg19405177
cg20784950
cg01870834
cg24891660
cg14598846
cg23299254
cg07427475
cg04255391
cg02331830
cg10299941
chr8:
145,002,000
145,004,000
145,006,000
145,008,000
C
cg21511203 + 6.2kb
cg07212837 + 62kb
rs11780978 +22kb

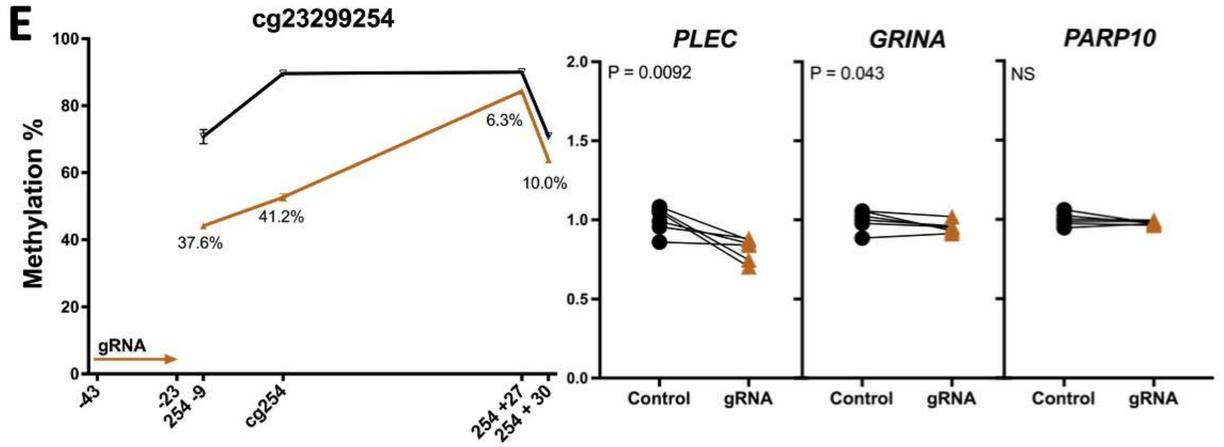

cg07427475
n = 25 P = 0.0001
Methylation (%)
G/G
A/G
A/A
TC28
iASCs9
cg19405177
n = 29 P = 0.0024
cg02331830
n = 21 P = 0.0039
cg1488846
n = 20 P = 0.0011
cg21511203
n = 24 P = 0.0076
cg23299254
n = 38 P = <0.0001

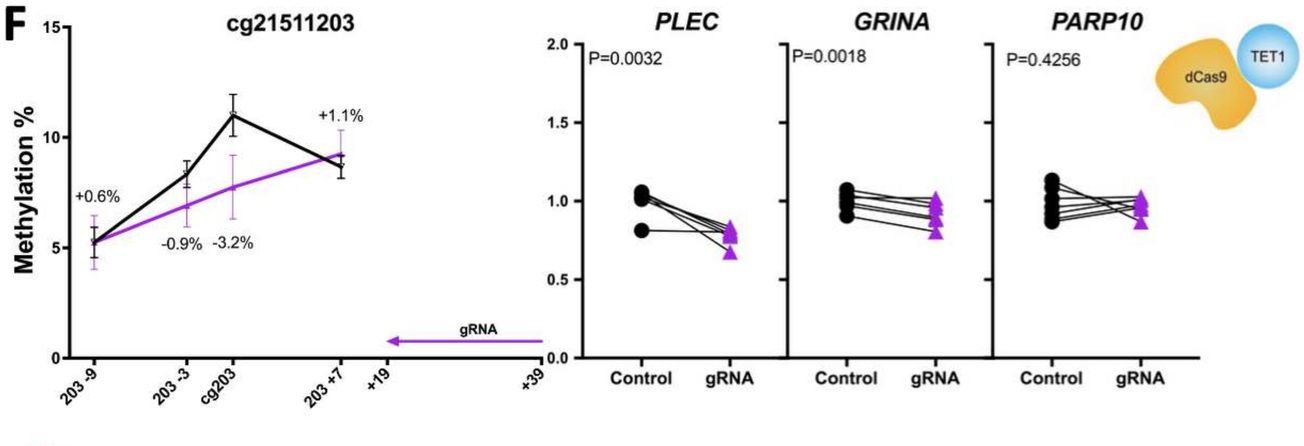

A
cg19405177
Methylation %
8.0%
12.5%
10.5%
16.3%
33.1%
1.9%
2.6%
0.3%
gRNA
177 -67
177 -50
177 -44
177 -22
cg177
177 +16
+24
177 +36
+44
177 +57
PLEC
GRINA
PARP10
NS
P = 0.013
P = 0.019
Control
gRNA

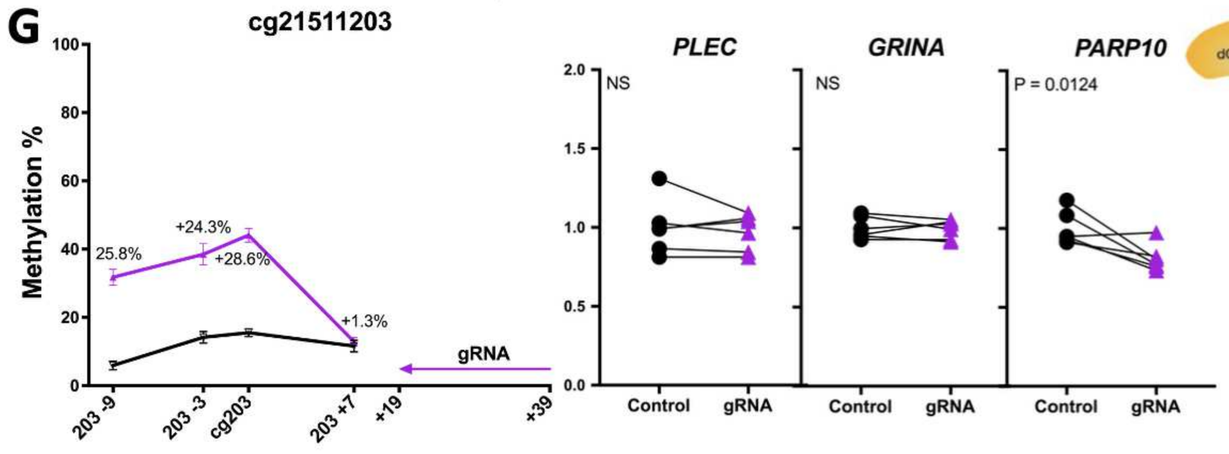

B
cg07427475
Methylation %
gRNA
-40
-20
cg475
5.8%
PLEC
GRINA
PARP10
NS
P = 0.035
P = 0.0005
dCas9
TET1
Control
gRNA

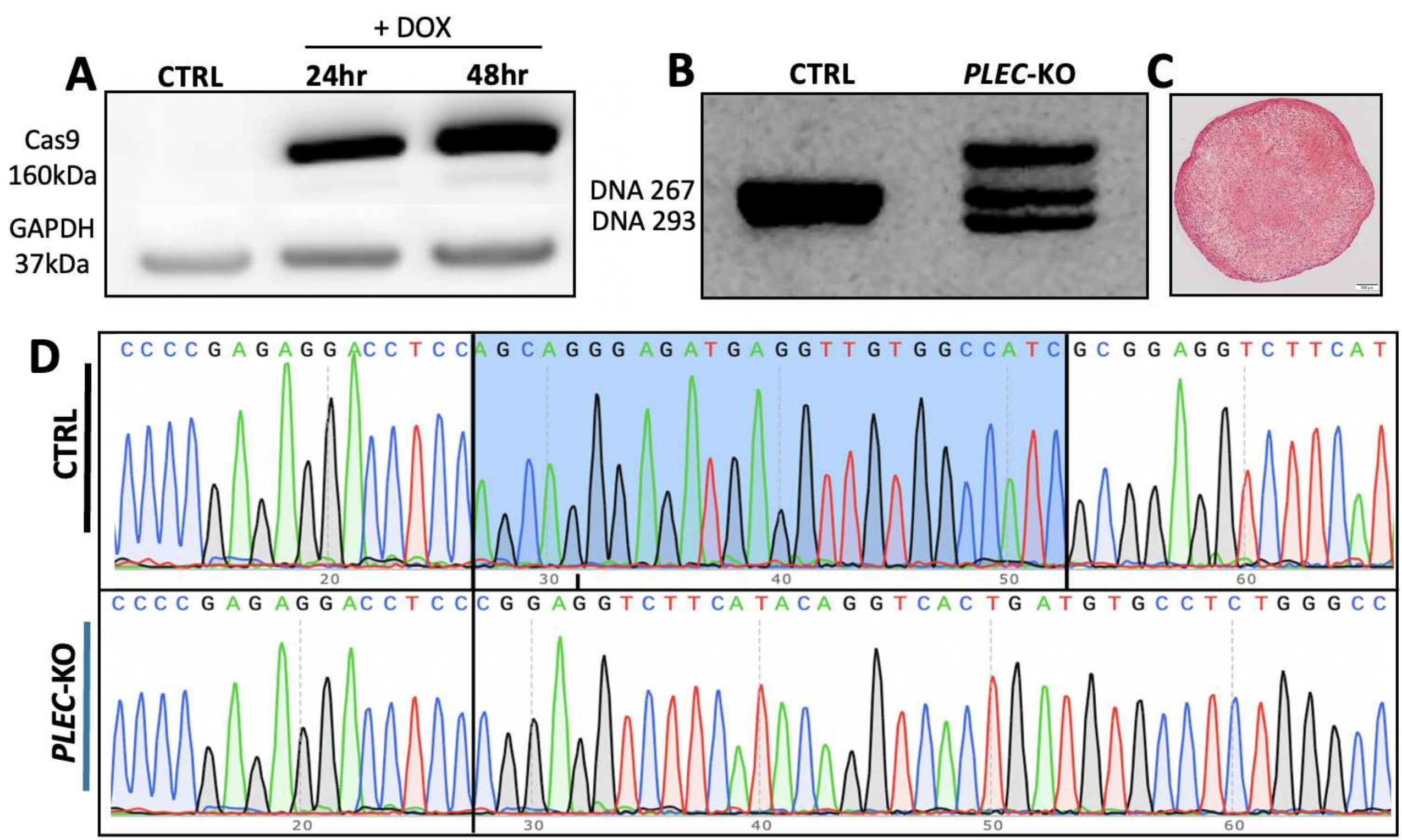

C
cg02331830
Methylation %
19.0%
18.1%
24.1%
gRNA
830 -2
cg830
830 +7
+24
+44
PLEC
GRINA
PARP10
NS
P = 0.09
NS
Control
gRNA

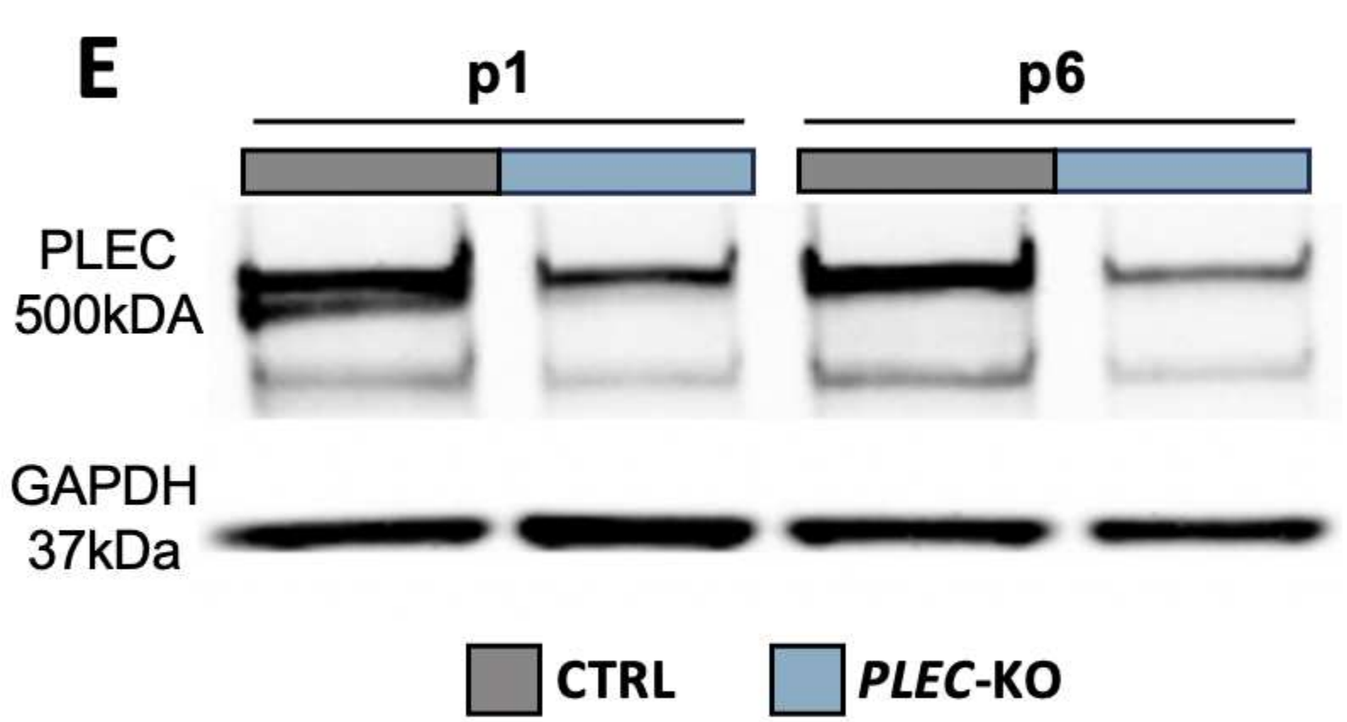

D
cg14598846
Methylation %
19.3%
15.1%
9.2%
9.5%
gRNA
-51
-31
cg846
846 + 9
846+18
846 +21
PLEC
PARP10
GRINA
P = 0.0014
NS
P = 0.0116
dCas9
TET1
Control
gRNA

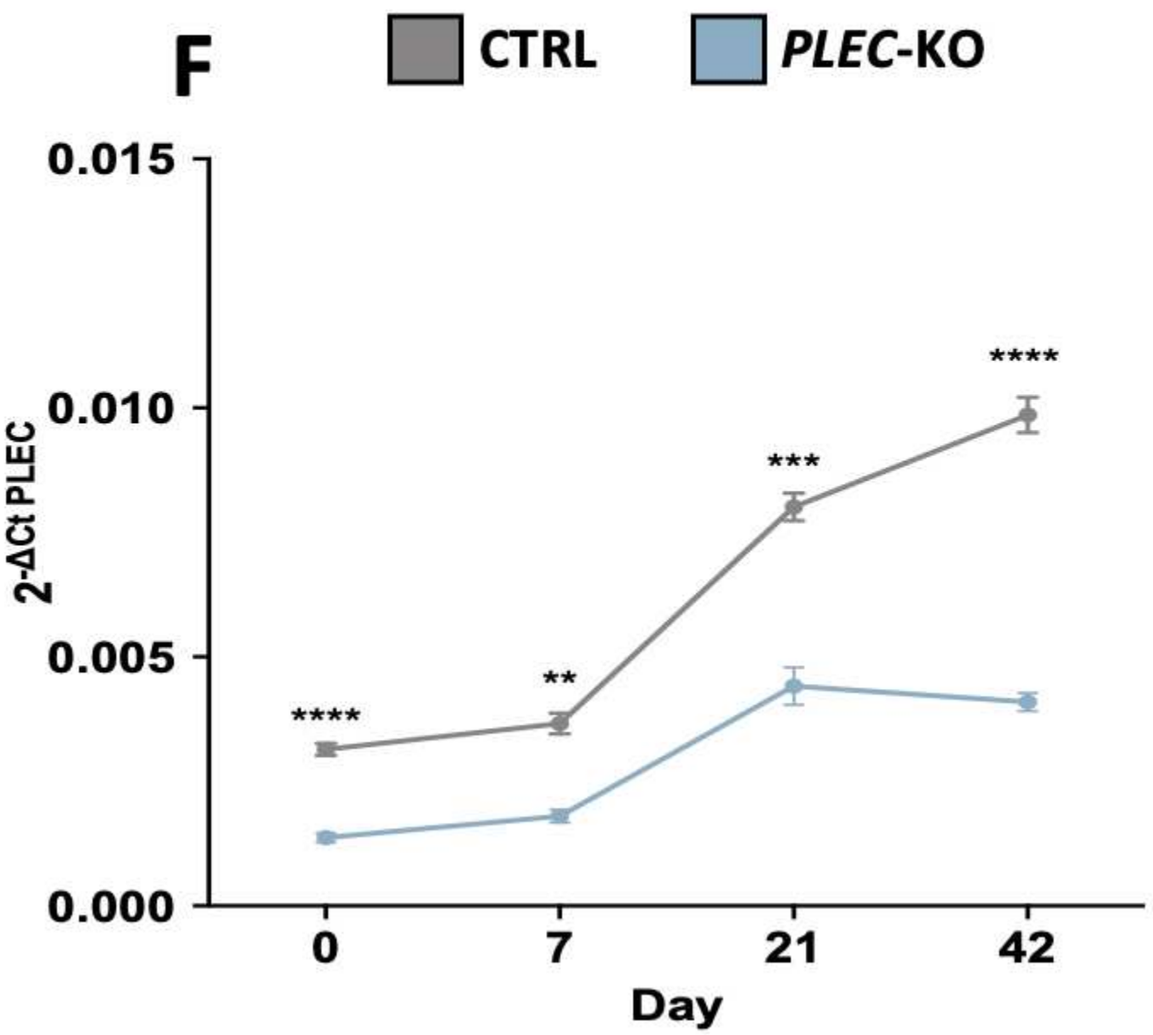

E
cg23299254
Methylation %
37.6%
41.2%
6.3%
10.0%
gRNA
-43
-23
254 -9
cg254
254 +27
254 + 30
PLEC
GRINA
PARP10
P = 0.0092
P = 0.043
NS
Control
gRNA


F
cg21511203
Methylation %
+0.6%
-0.9%
-3.2%
+1.1%
gRNA
203 -9
203 -3
cg203
203 +7
+19
+39
PLEC
GRINA
PARP10
P=0.0032
P=0.0018
P=0.4256
dCas9
TET1
Control
gRNA

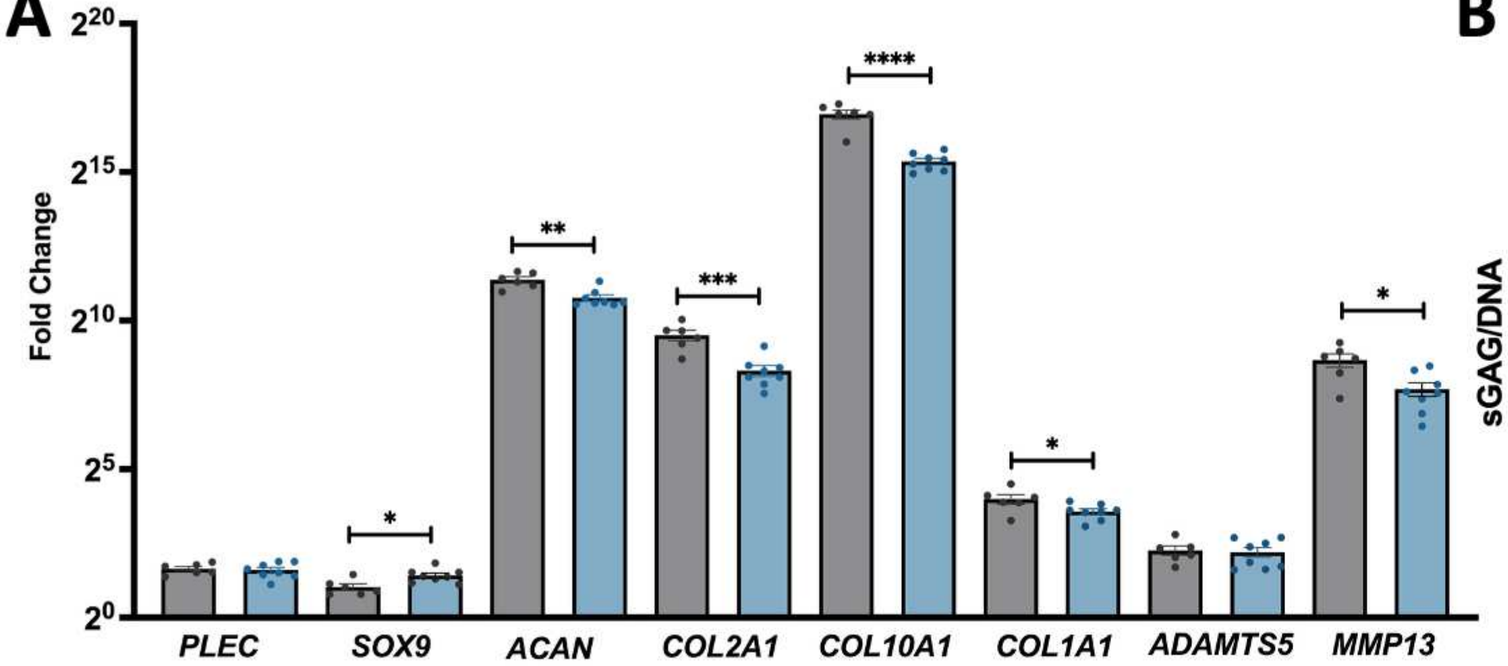

G
cg21511203
Methylation %
25.8%
+24.3%
+28.6%
+1.3%
gRNA
203 -9
203 -3
cg203
203 +7
+19
+39
PLEC
GRINA
PARP10
NS
NS
P = 0.0124
dCas9
DNMT3a
Control
gRNA


A
+ DOX
CTRL
24hr
48hr
Cas9
160kDa
GAPDH
37kDa
B
CTRL
PLEC-KO
DNA 267
DNA 293
C
D
CTRL
PLEC-KO
CCCCGAGAGGACCTCC
AGCAGGGAGATGAGGTTGTGGCCATC
GCGGAGGTCTTCAT
CGGAGGTCTTCATACAGGTCACTGATGTGCCTCTGGGCC
20
30
40
50
60

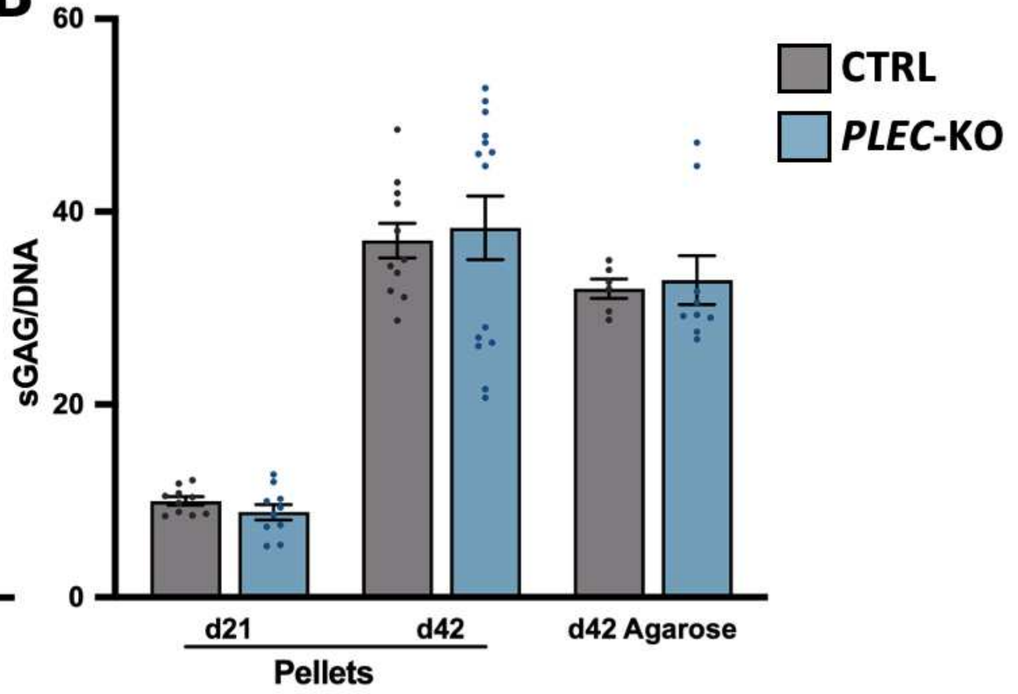

E
p1
p6
PLEC
500kDA
GAPDH
37kDa
CTRL
PLEC-KO


F
CTRL
PLEC-KO
2-ΔCt PLEC
0.015
0.010
0.005
0.000
****
**
***
****
0
7
21
42
Day

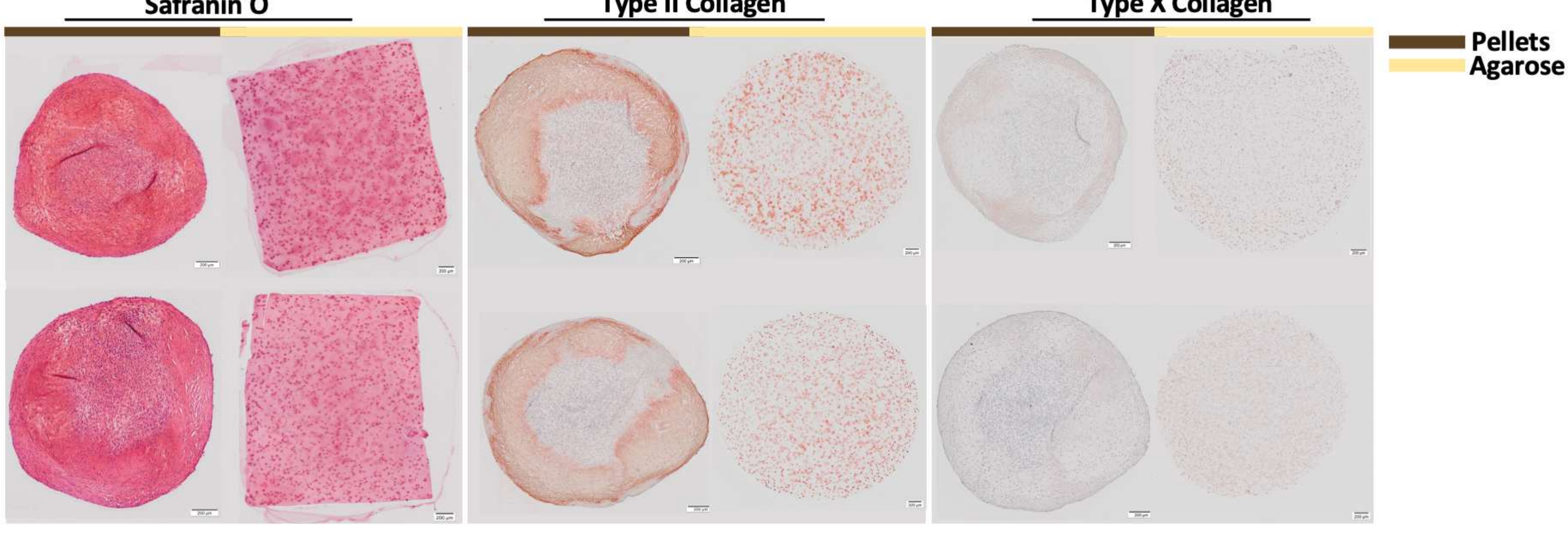
A


Fold Change
$2^{20}$
$2^{15}$
$2^{10}$
$2^{5}$
$2^{0}$
*
**
***
****
*
*
*
PLEC
SOX9
ACAN
COL2A1
COL10A1
COL1A1
ADAMTS5
MMP13

B


sGAG/DNA
60
40
20
0
CTRL
PLEC-KO
d21
d42
d42 Agarose
Pellets

C


Safranin O
Type II Collagen
Type X Collagen
CTRL
PLEC-KO
Pellets
Agarose

A

Chondrocyte Height (µm)

20
15
10
5
0

ns

n = 103-115

CTRL

*PLEC*-KO

B

Chondrocyte Deformation (%)

150
100
50
0

ns

n = 103-115

CTRL

*PLEC*-KO

C

Max 340/380 $Ca^{2+}$ ratio

0.6
0.4
0.2
0
-0.2

n = 106-116

CTRL

*PLEC*-KO

D

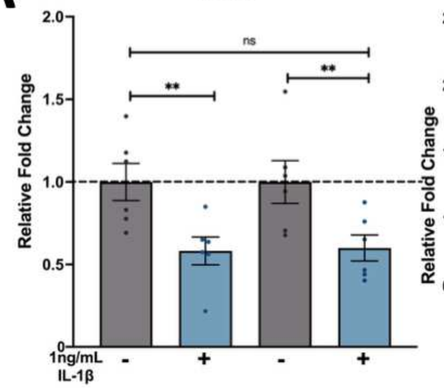
% Responders

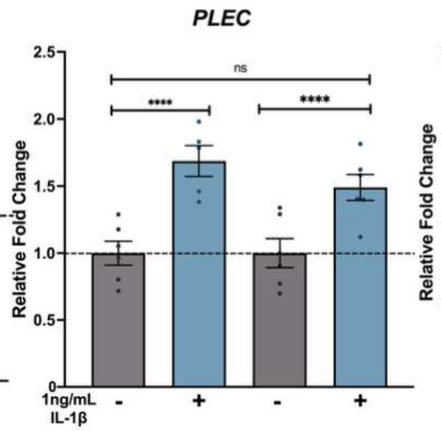
25
20
15
10
5
0

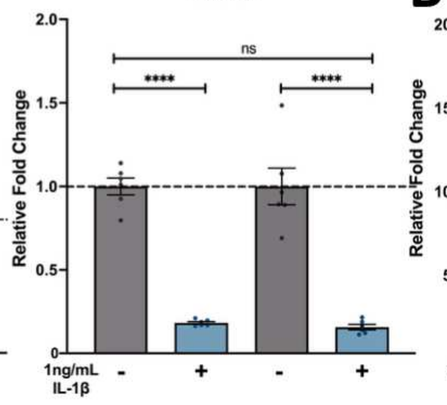
CTRL

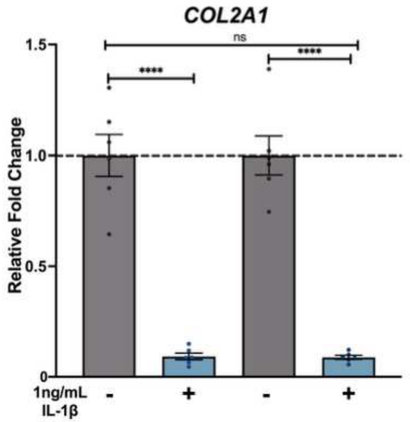
*PLEC*-KO

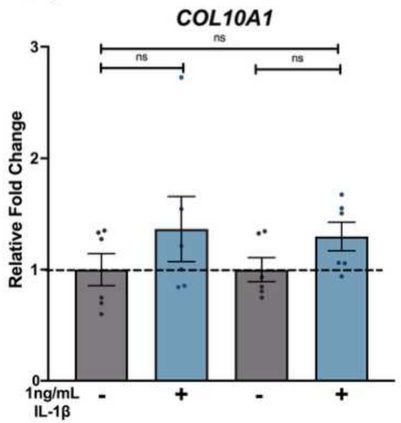
A


SOX9
Relative Fold Change
2.0
1.5
1.0
0.5
0
ns
**
**
1ng/mL
IL-1β
-
+
-
+

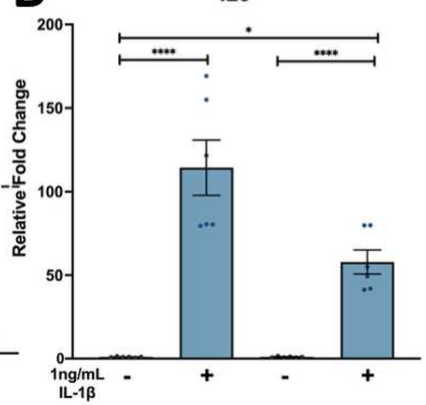

PLEC
Relative Fold Change
2.5
2.0
1.5
1.0
0.5
0
ns
****
****
1ng/mL
IL-1β
-
+
-
+

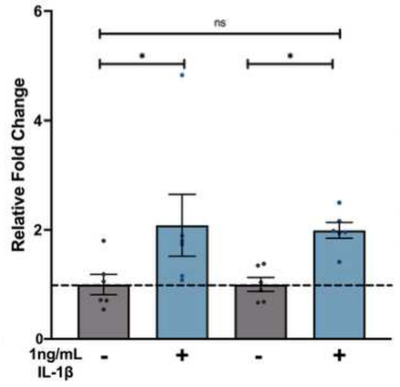

ACAN
Relative Fold Change
2.0
1.5
1.0
0.5
0
ns
****
****
1ng/mL
IL-1β
-
+
-
+

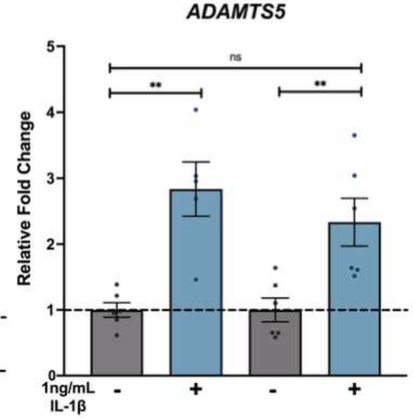

COL2A1
Relative Fold Change
1.5
1.0
0.5
0
ns
****
****
1ng/mL
IL-1β
-
+
-
+


COL10A1
Relative Fold Change
3
2
1
0
ns
ns
ns
1ng/mL
IL-1β
-
+
-
+

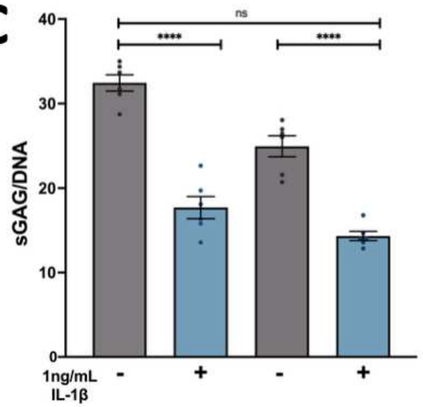
B


IL6
Relative Fold Change
200
150
100
50
0
*
****
****
1ng/mL
IL-1β
-
+
-
+


MMP13
Relative Fold Change
6
4
2
0
ns
*
*
1ng/mL
IL-1β
-
+
-
+

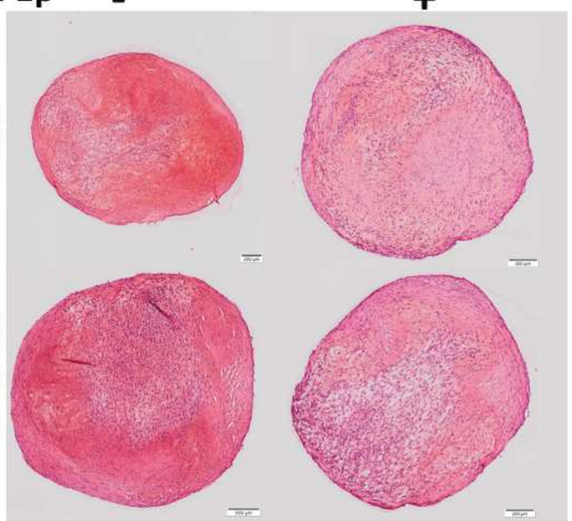

ADAMTS5
Relative Fold Change
5
4
3
2
1
0
ns
**
**
1ng/mL
IL-1β
-
+
-
+

C

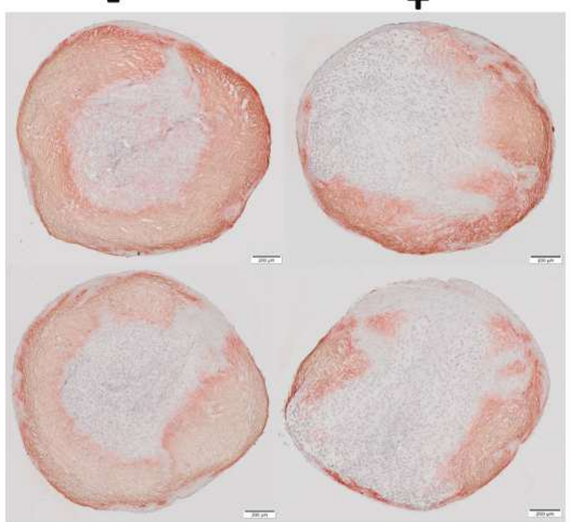

sGAG/DNA
40
30
20
10
0
ns
****
****
1ng/mL
IL-1β
-
+
-
+


CTRL
PLEC-KO

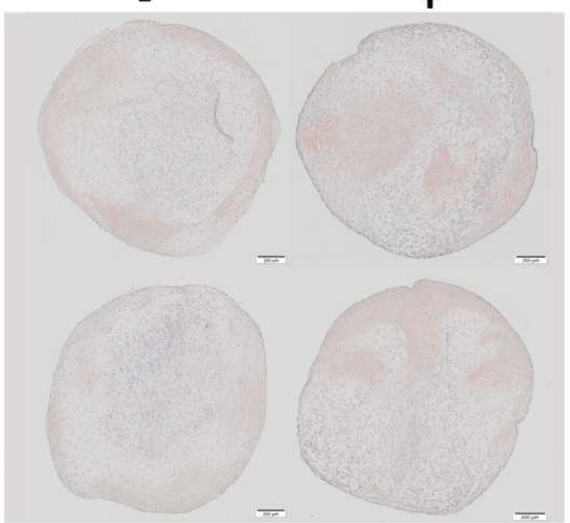
D


Safranin O
IL-1β
-
+
CTRL
PLEC-KO

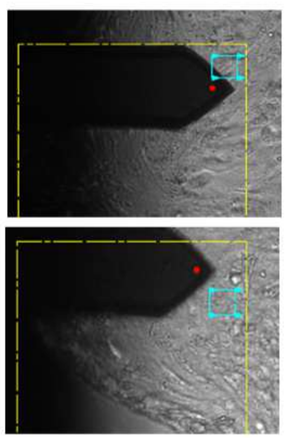
E


Type II Collagen
-
+

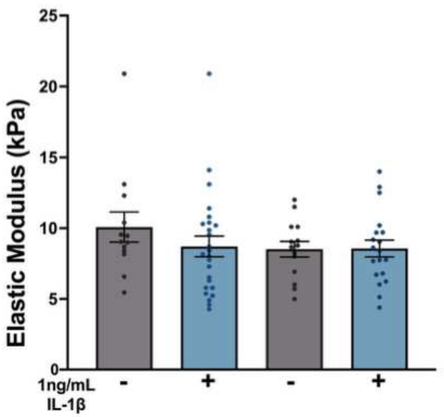
F


Type X Collagen
-
+

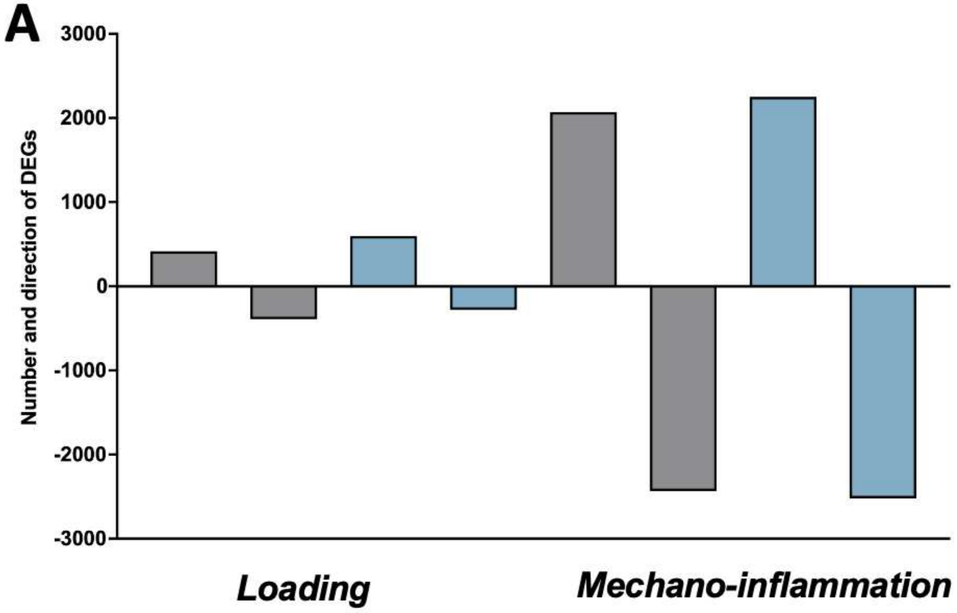
G



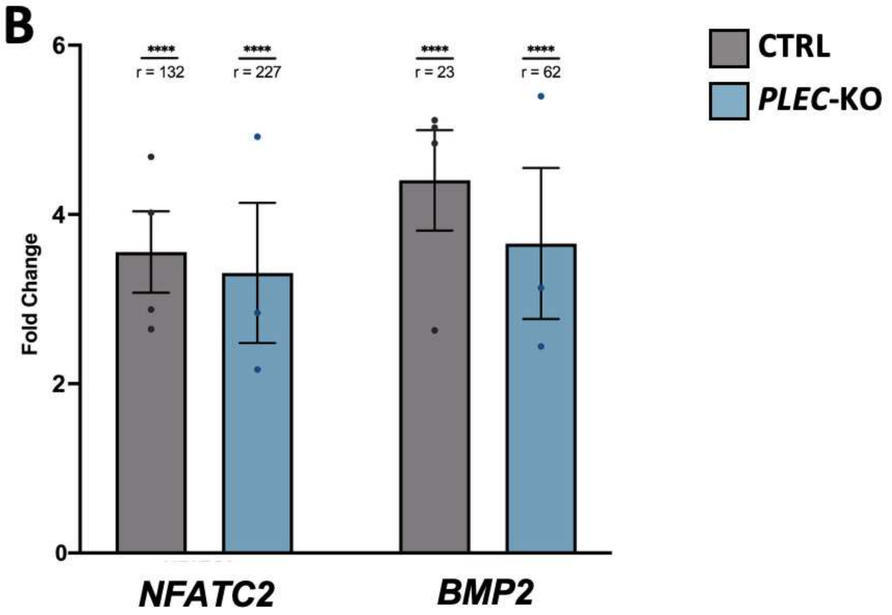
H


Elastic Modulus (kPa)
25
20
15
10
5
0
1ng/mL
IL-1β
-
+
-
+

**A**




**B**




**C**

Top Ranked KIR Genes in response to anabolic loading

| Rank | Gene | Mean CPM | pAdj (pKO 2 vs 1) | pKO 2 vs 1 (L2FC) | pC 2 vs 1 (L2FC) | pKO / pC (L2FC) | Rank | Gene | Mean CPM | pAdj (pKO 2 vs 1) | pKO 2 vs 1 (L2FC) | pC 2 vs 1 (L2FC) | pKO / pC (L2FC) |
|---|---|---|---|---|---|---|---|---|---|---|---|---|---|
| 1 | *TAGLN* | 20.93 | 4.08E-05 | 1.12 | 0.05 | 20.81 | 1 | *MGST1* | 24.35 | 9.81E-08 | -1.03 | -0.16 | -6.51 |
| 2 | *AC138028.2* | 21.61 | 2.27E-06 | 1.10 | 0.18 | 6.04 | 2 | *ENPP2* | 18.26 | 1.25E-02 | -1.19 | -0.34 | -3.53 |
| 3 | *LCAT* | 17.52 | 1.17E-05 | 1.05 | 0.46 | 2.29 | 3 | *ERI2* | 11.19 | 2.66E-08 | -1.37 | -0.51 | -2.71 |
| 4 | *AC245100.4* | 13.25 | 1.57E-05 | 1.09 | 0.47 | 2.29 | 4 | *LRRTM3* | 11.19 | 3.67E-04 | -1.03 | -0.39 | -2.64 |
| 5 | *AC104958.1* | 10.83 | 6.29E-04 | 1.04 | 0.47 | 2.20 | 5 | *STEAP1B* | 12.63 | 8.12E-05 | -1.00 | -0.38 | -2.63 |
| 6 | *RRN3P3* | 11.49 | 2.38E-05 | 1.28 | 0.70 | 1.83 | 6 | *STEAP1* | 10.00 | 8.08E-05 | -1.23 | -0.47 | -2.62 |
| 7 | *PRKCA-AS1* | 11.78 | 2.53E-09 | 1.33 | 0.73 | 1.82 | 7 | *ZNF441* | 13.33 | 7.53E-03 | -1.05 | -0.42 | -2.49 |
| 8 | *AL358216.1* | 15.03 | 9.92E-05 | 1.11 | 0.61 | 1.82 | 8 | *SORD* | 12.31 | 1.71E-06 | -1.18 | -0.50 | -2.37 |
| 9 | *AC016831.1* | 24.05 | 1.28E-04 | 1.33 | 0.75 | 1.77 | 9 | *PIR* | 14.24 | 7.63E-08 | -1.06 | -0.45 | -2.35 |
| 10 | *PER2* | 36.70 | 5.55E-06 | 1.13 | 0.73 | 1.55 | 10 | *PER3* | 10.27 | 1.09E-02 | -1.11 | -0.48 | -2.32 |

**D**

Top Ranked KIR Genes in response to anabolic loading in the presence of inflammation

| Rank | Gene | Mean CPM | pAdj (pKO 2 vs 1) | pKO 2 vs 1 (L2FC) | pC 2 vs 1 (L2FC) | pKO / pC (L2FC) | Rank | Gene | Mean CPM | pAdj (pKO 2 vs 1) | pKO 2 vs 1 (L2FC) | pC 2 vs 1 (L2FC) | pKO / pC (L2FC) |
|---|---|---|---|---|---|---|---|---|---|---|---|---|---|
| 1 | *SPTBN5* | 72.70 | 3.38E-14 | 1.14 | 0.73 | 1.55 | 1 | *COL1A1* | 167.89 | 9.32E-03 | -1.12 | 0.18 | -6.16 |
| 2 | *CITED2* | 19.45 | 5.77E-07 | 1.21 | 0.93 | 1.31 | 2 | *H19* | 12.17 | 2.27E-02 | -1.45 | -0.64 | -2.25 |
| 3 | *EIF4A1* | 10.17 | 1.06E-05 | 1.09 | 0.85 | 1.28 | 3 | *CSF2* | 8.97 | 3.63E-02 | -1.01 | -0.55 | -1.82 |
| 4 | *THUMPD3-AS1* | 23.03 | 4.85E-10 | 1.01 | 0.80 | 1.27 | 4 | *PIM2* | 17.79 | 4.59E-09 | -1.28 | -0.86 | -1.50 |
| 5 | *CRADD* | 20.79 | 4.23E-08 | 1.14 | 0.91 | 1.25 | 5 | *RASSF5* | 16.93 | 1.27E-10 | -1.21 | -0.83 | -1.46 |
| 6 | *AC090673.1* | 92.17 | 1.40E-05 | 1.04 | 0.85 | 1.23 | 6 | *FRK* | 31.09 | 1.20E-05 | -1.18 | -0.91 | -1.29 |
| 7 | *ZNF860* | 12.40 | 9.61E-16 | 1.11 | 0.91 | 1.22 | 7 | *IP6K3* | 60.94 | 6.49E-11 | -1.02 | -0.82 | -1.25 |
| 8 | *FOXL1* | 31.32 | 9.35E-11 | 1.09 | 0.92 | 1.19 | 8 | *ARRDC3* | 215.51 | 3.91E-16 | -1.15 | -0.98 | -1.17 |
| 9 | *C11orf96* | 511.34 | 4.86E-04 | 1.12 | 0.94 | 1.19 | 9 | *TNFRSF1B* | 48.70 | 1.79E-09 | -1.06 | -0.98 | -1.08 |
| 10 | *MAFF* | 80.01 | 2.09E-25 | 1.10 | 0.93 | 1.18 | 10 | *BCL7A* | 9.06 | 4.63E-08 | -1.01 | -0.99 | -1.01 |

## Supplementary Files

This is a list of supplementary files associated with this preprint. Click to download.

- ARTSorialSupplemental25626.pptx